CHALMERS

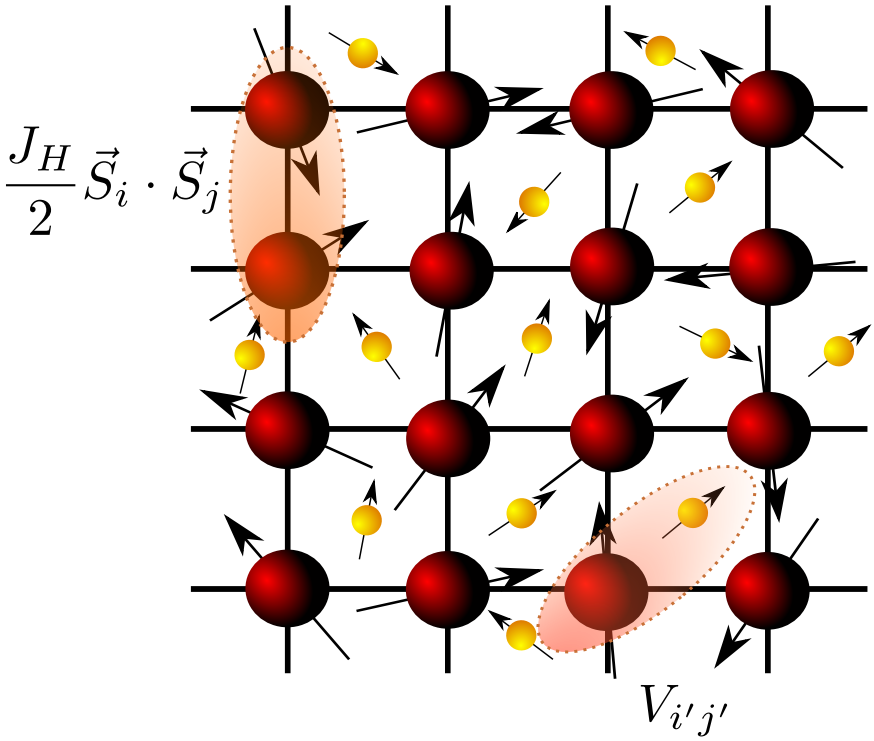

Tunneling into a Heavy Fermion System

Master of Science Thesis in Fundamental Physics

CHRISTIAN SPÅNSLÄTT

Department of Microtechnology and Nanoscience
Applied Quantum Physics Laboratory
Chalmers University of Technology
Göteborg, Sweden 2012

THESIS FOR THE DEGREE OF MASTER OF SCIENCE

Tunneling into a Heavy Fermion System

CHRISTIAN SPÅNSLÄTT

CHALMERS

Applied Quantum Physics Laboratory
Department of Microtechnology and Nanoscience
CHALMERS UNIVERSITY OF TECHNOLOGY
Göteborg, Sweden 2012

Tunneling into a Heavy Fermion System

CHRISTIAN SPÅNSLÄTT

Applied Quantum Physics Laboratory
Department of Microtechnology and Nanoscience
Chalmers University of Technology
SE-412 96 Göteborg, Sweden
Telephone +46(0)31-772 10 00

Cover illustration: *A conceptual picture of the Kondo lattice model on a two-dimensional square lattice. The red balls describe localized magnetic moments placed at the lattice sites, while the yellow balls represent conduction electrons. Magnetic moments interact among themselves with interaction strength J_H and itinerant electrons hybridize with the magnetic moments by the interaction V_{ij}.*

Printed at Chalmers Reproservice
Göteborg, Sweden 2012

Tunneling into a Heavy Fermion System

CHRISTIAN SPÅNSLÄTT
Applied Quantum Physics Laboratory
Department of Microtechnology and Nanoscience
Chalmers University of Technology
Göteborg, Sweden 2012

Abstract

The discovery of an extremely high effective electron mass in $CeAl_3$ by Andres et al in 1975 was the starting point for Heavy Fermion physics. One possible theory for explaining this heavy fermion behaviour is the Kondo lattice model which is investigated in this master thesis. With a slave boson mean field approach using Green's functions, a set of mean field equations are derived and solved. The solutions of these equations determine the model behaviour as a function of various input parameters. In addition, a system where the Kondo lattice model is in close proximity to a Scanning Tunneling Microscope is considered. By the use of non-equilibrium Keldysh formalism, a tunneling current and differential conductance is calculated. The differential conductance is seen to map out the Kondo lattice density of states.

Keywords: Heavy fermion, Kondo lattice, mean field theory, slave boson, Green's function, Scanning Tunneling Spectroscopy, differential conductance

Acknowledgements

It is my pleasure to thank those who have made this thesis possible. First of all, I want to thank my supervisor Mikael Fogelström for support and helpful discussions. I would also like to thank everybody else at the Applied Quantum Physics Laboratory for letting me be a part of your group and for the relaxing and motivating atmosphere you all generate.

Secondly, I'd like to thank Andreas for always being available to help with numerics and programming. Your support is invaluable!

I owe also a big thanks to Henrik Johannesson for introducing me to the exciting realm of quantum matter. Your courses I have taken have hooked me into this amazing field of physics.

I also want to thank Elin and Erik for your thorough proofreading. Your help is very appreciated!

My time here at Chalmers has been an amazing time, and apart from interesting studies it has mainly been due to my wonderful class mates. I want to give special thanks to Andreas, Olov and Stefan for all collaboration and happy times during the past five years and hopefully for the years to come as well.

Finally, I would also like to thank all my room mates; Elin, Eric, Erik, Viktor and David for all the good times together and for making the time studying a wonderful chapter of my life!

Christian Spånslätt, Göteborg, August 9, 2012

Contents

1

Introduction

One of the greatest triumphs of modern theoretical physics has been the **reductionism principle**. The main key of this philosophy is the idea that by knowledge about the constituent parts of a system, it can be modelled in an accurate way. High energy physicists and string theorists who in their quest for grand unified theories, theories aiming to explain the plethora of particles and four known fundamental interactions in our universe, are highly motivated by the reductionism principle.

However, during the nineteenth and twentieth century, by the introduction of statistical mechanics, it has become apparent that systems containing large numbers of particles exhibit fundamentally new properties - properties that could not be expected from the well known laws that rule the individual particles. This insight has been well summarized by P.W. Anderson who in a well-cited article [1] pin-pointed the concept into the following sentence:

More is different

It has also become apparent that not only number, but energy and dimensional scales, all contribute to the development of new and fascinating system properties. As an example, the microscopic theory of conventional superconductivity, the BCS-theory (named after its inventors Bardeen, Cooper and Schreiffer), explains the formation of dissipationless electrical currents in certain metals at low temperatures by electrical Coulomb *attraction* between electrons. Since the Coulomb force normally is *repulsive* between equal charges, it is not until the metal is sufficiently cold that the positive ions in the crystal lattice can participate in mediating an attractive interaction between the electrons. The formation of attracted electron pairs, **Cooper-pairs**, is the basic condition for the rise of the remarkable properties of a superconductor. The well understood Coulomb interaction

allows the system to exhibit new non-expected phenomena simply because scales (in this case the temperature scale) have changed.

The description above can be classified as phenomena of **holism** or **emergence**, the idea that natural systems sometimes must be viewed as a whole, rather than consisting of a collection of parts. For an instructive discussion on holism, see [2].

The description of a system containing great numbers of electrons at low temperatures is usually given by the Fermi liquid theory. This framework treats interacting electrons as non-interacting **quasiparticles**, electrons with renormalized dynamical properties such as mass or magnetic moment [3]. Although the Fermi liquid theory has been very successful, there are classes of systems where the theory breaks down. One class of such systems is called **strongly correlated electron systems**, where the interaction energy between electrons is by far greater than their kinetic energy. The strongly correlated electron systems constitute a wide class of physical systems that exhibit many interesting electronic and magnetic phenomena such as unconventional superconductivity, metal-insulator transitions, the Kondo effect and quantum hall effects.

There is a huge research effort in the understanding of these systems. Both from pure curiosity but also since the development of techniques for fabricating low dimensional nano-structures has made it possible to realize these strongly correlated systems in a laboratory. By exploiting the effects arising from strong electron interaction there is a possibility that completely new electronic devices and materials can be fabricated.

1.1 Heavy fermion systems

Andres, Graebner and Ott made a remarkable discovery in 1975 [4]. Measurements of the low temperature specific heat in $CeAl_3$ revealed electronic effective masses of more than a hundred times the ordinary electron mass. Some years later, in 1979, Steglich, Aarts, Bredl, Lieke, Meschede, Franz and Schäfer found a superconducting state in $CeCu_2Si_2$, a material which also showed a large electron effective mass [5]. Steglich et al coined the property of large electron mass **heavy fermion behaviour**.

However, apart from the heavy fermion behaviour, the superconducting state they had found was remarkable in the sense that $CeCu_2Si_2$ is a paramagnetic material. Until the discovery that Steglich et al made, superconductivity was considered impossible for magnetic materials. Since magnetic moments in these materials breaks time-reversal symmetry, the Cooper-pairs would become unstable due to spin-flipping scattering on the moments and the superconductivity would be suppressed.

These discoveries made a big impact since this unconventional superconductivity could not be explained by the BCS-theory and could be originating from a pairing-mechanism different from the phonon-mediated one. Later, the discovery of high temperature superconductivity, [6], would intensify the pursuit for this unknown pairing mechanism.

Studying heavy fermion systems, could therefore improve the understanding of one of the most important unsolved problems of condensed matter physics, high temperature superconductivity.

Since Andres et al and Steglich et al, many more condensed matter systems displaying the heavy fermion behaviour have been discovered. The common feature of the systems is that they are compounds containing rare-earth metals such as cerium or ytterbium and actinides like uranium or plutonium [7]. Although these metal compounds commonly display heavy fermion behaviour, they also exhibit various different properties such as superconductivity, anti-ferromagnetism and insulator behaviour.

One reason for the increased research of these heavy fermion systems is that it have been apparent that by external pressure and magnetic fields, it is possible to drive transitions between anti-ferromagnetism and heavy fermion behaviour [8]. This transition is called a **quantum critical point** and was discovered in 1995 [9]. Apart from fundamentally interesting, the heavy fermion systems may be suitable for creating new devices exploiting the materials exotic behaviour. For further reading about heavy fermion systems, consider [8, 10, 11].

Andres et al suggested that a lattice version of the **Kondo effect** might be responsible for the heavy fermion behaviour. To understand what this means, a brief discussion of magnetic moments and the Kondo effect is given below.

1.2 Anderson formation of magnetic moments

This discussion follows the work of [8]. In order to understand the physics that governs the Kondo lattice it is crucial to understand why magnetic moments arise in the atoms building the lattice. The most used model for describing the formation of magnetic moments is the **Anderson model**:

$$H = \sum_{k\sigma} \epsilon_k c^\dagger_{k\sigma} c_{k\sigma} + \epsilon_f n_f + U n_{f\uparrow} n_{f\downarrow} + \sum_{k\sigma} V_{k\sigma} \left[f^\dagger_\sigma c_{k\sigma} + c^\dagger_{k\sigma} f_\sigma \right]. \tag{1.1}$$

The first term describes a conduction electron band, the second and third an ion with localized f-electrons and the last term describes hybridization between the c- and f-electron states. This Hamiltonian models a system of two f-electron states in an atom hybridizing with an embedding sea of conduction electrons.

Considering the atom part of the Hamiltonian

$$H_{atom} = \epsilon_f n_f + U n_{f\uparrow} n_{f\downarrow}, \tag{1.2}$$

where there are four possible quantum states: $|f^0\rangle$, $|f^2\rangle$, which are non-magnetic since there is no net spin in any of the states.

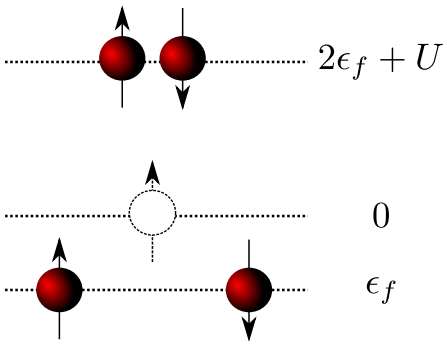

Figure 1.1: *The figure shows the four different states of the f-orbital with their respective energies. The states that are magnetic are the ones with a single occupancy.*

The magnetic states are $|f^1 \uparrow\rangle$ and $|f^1 \downarrow\rangle$, where there is a net spin due to the single occupation. See figure 1.1. When calculating the energy of these states one finds that:

$$\begin{aligned} E(f^0) &= 0, \\ E(f^2) &= 2\epsilon_f + U, \\ E(f^1) &= \epsilon_f. \end{aligned} \tag{1.3}$$

If the groundstate is magnetic, the cost for removing or adding an electron in the f-orbital is given by:

$$\begin{aligned} \text{removing:} \quad & E(f^0) - E(f^1) = -\epsilon_f > 0, \\ \text{adding:} \quad & E(f^2) - E(f^1) = \epsilon_f + U > 0. \end{aligned} \tag{1.4}$$

The difference between these energies $\Delta E = U/2 \pm (\epsilon_f + U/2)$ gives the condition for keeping the local moment: provided that

$$U/2 > |\epsilon_f + U/2| \tag{1.5}$$

the energy is lowest when there is one single electron in the orbital, and thus a non-zero spin - a magnetic moment. As can be seen in equation 1.5, the criteria is fulfilled for large U. There is yet another requirement for keeping the local moment, that the surrounding temperature is of the scale $k_B T < \max(\epsilon_f + U, -\epsilon_f)$ so that no thermal excitations may break the single occupancy of the orbital. For an ion of this kind inserted in a sea of conduction electrons, some spectacular effects can take place. This is the topic of the next section below.

1.3 The Kondo effect

In a normal metal, the behaviour of the conduction electrons is well described by Landau's theory of Fermi liquids. This theory predicts that when the temperature, T, decreases, the electrical resistance, ρ, of the metal will drop according to

$$\rho(T) = \rho_0 + aT^2 + bT^5 \tag{1.6}$$

for small T . The constant zero temperature resistance, ρ_0, is mainly due to impurities and defects of the metal, the T^2-term, where a is some constant, describes scattering of electrons against other electrons and the bT^5- term describes electron-phonon scattering, where b is an another constant.

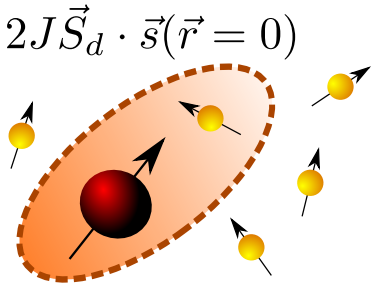

Figure 1.2: *The figure shows the Kondo interaction. The magnetic moment, depicted in red, is situated at $\vec{r} = 0$ and interacts with the spins of surrounding conduction electrons with an interaction of strength J.*

However, when some metals are doped with impurities having magnetic moments, the temperature dependence of the resistance changes for decreasing T. Instead of converging to a constant value as above, the resistance increases again below some specific temperature, T_{min}, and stops at a finite value at $T = 0$. In other words, a resistivity minimum arises [12].

This phenomenon is named after the Japanese physicist Jun Kondo, who in 1964 was the first to explain the origin of the resistance minimum [13]. His approach was second order perturbation theory on the so called **sd-Hamiltonian**,

$$H_{sd} = \sum_{k,\sigma} \epsilon_k c^\dagger_{k\sigma} c_{k\sigma} + J\vec{S}_d \cdot \sum_{kk'\sigma\sigma'} c^\dagger_{k\sigma} \vec{\sigma}_{\sigma\sigma'} c_{k'\sigma'} \tag{1.7}$$

which describes a free magnetic moment, $\vec{S}_d$ at $\vec{r} = 0$ interacting with a conduction electron sea, see figure 1.2. He could then argue that the increase in resistance below T_{min} is due to electron spin-flip scattering events against the inserted magnetic impurities. This is called the Kondo effect. Kondo showed that these events changes the resistance low temperature dependence to

$$\rho(T) = \rho_0 + c \ln \frac{\mu}{T} + bT^5 \tag{1.8}$$

where c and μ are additional constants. This additional logarithmic term will produce a minimum resistivity $T_{min} = (\frac{c}{5b})^{\frac{1}{5}}$ which agrees very well with experiments [13].

Although Kondo could explain the resistivity minimum, a problem in his model immediately developed. The logarithmic term is divergent as T goes to zero. Therefore the Kondo model could not be valid for extremely low temperatures. Additional work and calculations by Wilson, using **renormalization group** methods, could modify the theory to give a finite value at $T = 0$ [14]. Kondo's model is thus only valid high above a certain temperature, the Kondo temperature T_k. This Kondo temperature is also the temperature at which the impurity and conduction electrons spins begin to condensate into singlet states. These states will modify the density of states spectrum, by a so called Kondo resonance, which is manifested by a temperature dependent peak at the Fermi level in the spectrum.

1.4 Scanning Tunneling Spectroscopy

Scanning Tunneling Spectroscopy, **STS**, is an experimental technique for acquiring information about a materials local density of states, **LDOS** [15]. As a simplified conceptual setup, consider an extremely thin metal tip that is put at a certain height above a sample to be investigated, see figure 1.3. If the metal tip is sufficiently close to the sample, the electron wave functions of the tip begin to overlap with the wave functions in the sample. By applying a voltage between the tip and the sample, a tunneling current will develop. The simplest information that can be obtained is this current as a function of the voltage which determine how many electrons that are allowed to tunnel. Under certain ideal circumstances, such as low temperature, low noise and low energy dependence on the wavefunction overlap matrix elements, the current as a function of voltage is approximately given by:

$$I \propto \int_0^{eV} D_{tip}(\epsilon - eV) D_{sample}(\epsilon) d\epsilon \tag{1.9}$$

If the density of states, D, in the tip is approximately constant, a feature that is highly desirable, the **differential conductance** is given by

$$\frac{dI}{dV} \propto D_{sample}(\epsilon - eV) \tag{1.10}$$

and maps out the sample LDOS at the position of the tip. There are various other experimental techniques by using tunneling microscopy, but these are out of the scope of this thesis. For an instructive introduction to tunneling microscopy, see [15].

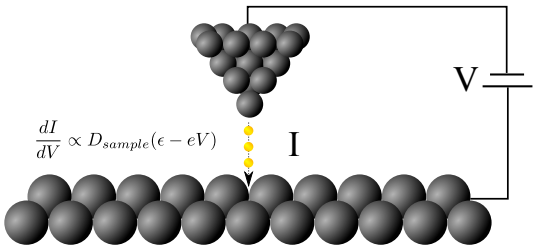

Figure 1.3: *The figure shows a simple STS-setup. An applied bias voltage between the tip and the sample will alter the tunneling current between them. The differential conductance, dI/dV maps under ideal circumstances out the sample local density of states.*

1.5 Objective and outline

There are two topics considered in this thesis. The first is the investigation of a **Kondo lattice model**, which is thought to be the underlying theory for a description of heavy fermion behaviour. Secondly, the Kondo lattice coupled to a metallic tunneling tip is investigated. By allowing electrons to tunnel from the tip into the lattice, a **tunneling current** and **differential conductance** can be calculated. This configuration is a simple model of a STS-setup.

The outline of the thesis is:

Chapter 2 - Theory Toolbox describes the theoretical framework required for solving the problems of this thesis. First, a brief introduction to **second quantization** is given followed by a description of **mean field theory** and the **pictures of quantum mechanics**. Then the concept of **Green's functions** is described, both in equilibrium and non-equilibrium where finally the **Keldysh formalism** is introduced.

Chapter 3 - The Kondo lattice contains the study of the first problem. With a **slave boson** mean field approach, the self consistency equations for the mean field parameters are derived, allowing for studies of the model behaviour as a function of various input parameters.

Chapter 4 - Tunneling into the Kondo lattice is devoted to the second problem. Here the non-equilibrium techniques are used to derive equations for the current and differential conductance of the tunneling process.

Chapter 5 - Results and conclusions presents and discusses the results of the two problems addressed in the two previous chapters.

Chapter 6 - Summary and outlook summarizes the thesis and discusses further progress in investigating the problems.

2

Theory toolbox

This chapter is devoted to the theoretical framework that underlines the work in this thesis. First, a quick introduction to the **second quantization** language is presented. This is the mathematical framework used in this thesis to describe quantum mechanics. Secondly a description of mean field theory, which is a procedure that greatly simplifies complex problems in condensed matter, is given followed by an overview of the pictures of quantum mechanics. These pictures are three different ways of treating time in quantum mechanics, of which the interaction picture is the one used in this thesis.

The main theoretical study for this thesis has been the understanding of **Green's functions**, both in thermal equilibrium at arbitrary temperatures but also in non-equilibrium. The former of these situations is well described by the **Matsubara Green function formalism** while the **Keldysh formalism** is suitable for the latter. A description of these topics follows.

2.1 Second quantization

This section closely follows and summarizes the most important parts of section 2.1 in [16]. Second quantization is a language of quantum mechanics based on the algebra of ladder operators and is suitable for dealing with many-body systems. Within the second quantization formalism, many body quantum states with N particles are described by "N-letter words" on the form

$$|4, 2, 1, 0, 7, 9, ...\rangle \tag{2.1}$$

where the ith number describes how many particles that occupy the single particle state i. For fermions, which obey the Pauli exclusion principle, the occupation numbers take only the value 0 or 1. This defines the **occupation number representation** where the basis states in the Hilbert space F^N, the space containing all N-particle states, are given by $|n_1, n_2, n_3, ...\rangle$. For a fixed number of particles, the equation $\sum_i n_i = N$ is fulfilled. Any state in F^N can be generated by a superposition of the basis states:

$$|\psi\rangle = \sum_{n_1,n_2,...} c_{n_1,n_2,...}|n_1, n_2, ...\rangle \tag{2.2}$$

with the constraint $\sum_i n_i = N$.

To relax the condition of a fixed number of particles, a Hilbert space big enough to household any number of particles has to be constructed. The space

$$F = \bigoplus_{N=0}^{\infty} F^N \tag{2.3}$$

will do the trick. This space is called the **Fock space** and contains F^0 which denotes the vacuum space, the part of the theory where no particles are present anywhere. This space has only one basis state which is denoted as $|0\rangle$ and is usually called the **vacuum**. The formation of states in the Fock space works just as before but the constraint can now be dropped, which means that a general state $|\psi\rangle$ can be a superposition of states containing different number of particles.

To extend the representation, a **creation**, $a_i^\dagger$, and an **annihilation operator** a_i are defined to each corresponding single particle state i. The operators are defined through:

$$a_i^\dagger|n_1, ..., n_i, ...\rangle \propto |n_1, ..., n_i + 1, ...\rangle. \tag{2.4}$$

By the repeated use of creation operators on the vacuum, every basis state in the Fock space can be obtained:

$$|n_1, n_2, ...\rangle = \prod_i \frac{1}{\sqrt{n_i!}}(a_i^\dagger)^n|0\rangle \tag{2.5}$$

Note, that since fermions can only occupy one state each, the action of a creation operator onto an already occupied state gives zero. The distinction between this fermionic behaviour and bosonic properties can remarkably simply be imposed by commutation relations for the two operator classes:

$$[a_i,a_j]_\zeta = 0, \quad [a_i^\dagger,a_j^\dagger]_\zeta = 0, \quad [a_i,a_j^\dagger]_\zeta = \delta_{ij} \tag{2.6}$$

where $[A,B]_\zeta = AB - \zeta BA$ is the commutator for bosons, $\zeta = 1$, and the anticommutator for fermions $\zeta = -1$. One very beneficial property of the second quantization language is that the symmetry between fermions and bosons is captured by the symmetry of these operator commutation relations.

To formulate quantum mechanics in the second quantization language, some more investigations must be done. The first one is to be able to transform between one single particle basis $\{\lambda\}$ to another, $\{\tilde{\lambda}\}$ and see what consequences this has on the operator algebra. By using the resolution of identity $\sum_\lambda |\lambda\rangle\langle\lambda|$ one can show that the transformation law is given by:

$$a_{\tilde{\lambda}}^\dagger = \sum_\lambda \langle\lambda|\tilde{\lambda}\rangle a_\lambda^\dagger, \quad a_{\tilde{\lambda}} = \sum_\lambda \langle\tilde{\lambda}|\lambda\rangle a_\lambda \tag{2.7}$$

For continuous sets of quantum numbers, such as position or momentum, the sums above translates to integrals. The commutation relations, equation 2.6, are preserved by the transformation law.

Next, the single particle operators are to be expressed in the second quantization language. These operators, $\hat{O}_1$, when acting in a N-particle Hilbert space F^N generally takes the form $\hat{O}_1 = \sum_{n=1}^N \hat{o}_n$ where $\hat{o}_n$ is a single particle operator, such as kinetic energy or an external scalar potential, acting on the nth particle. For the purpose of finding a representation of the single particle operator it is convenient to define the **number operator**

$$\hat{n}_\lambda = a_\lambda^\dagger a_\lambda \tag{2.8}$$

which simply counts the number of particles in the single particle state $|\lambda\rangle$.

Assuming that the operator $\hat{O}_1$ is diagonal in the basis $\{\lambda\}$, that is $\hat{O}_1 = \sum_i o_{\lambda_i} |\lambda_i\rangle\langle\lambda_i|$ with $o_{\lambda_i} = \langle\lambda_i|\hat{o}|\lambda_i\rangle$. Then for one particular number of particles

$$\begin{aligned}\langle n'_{\lambda_1}, n'_{\lambda_2}, ...|\hat{O}_1|n'_{\lambda_1}, n'_{\lambda_2}, ...\rangle &= \sum_i o_{\lambda_i} n_{\lambda_i} \langle n'_{\lambda_1}, n'_{\lambda_2}, ...|n'_{\lambda_1}, n'_{\lambda_2}, ...\rangle \\ &= \langle n'_{\lambda_1}, n'_{\lambda_2}, ...| \sum_i o_{\lambda_i} \hat{n}_{\lambda_i} |n'_{\lambda_1}, n'_{\lambda_2}, ...\rangle \end{aligned} \tag{2.9}$$

Utilizing this result to a state with any number of sets of states the operator can be generalized to

$$\hat{O}_1 = \sum_\lambda o_\lambda \hat{n}_\lambda = \sum_\lambda o_\lambda a_\lambda^\dagger a_\lambda. \tag{2.10}$$

The interpretation of this formulation is that the operator simply counts the number of particles in the state $|\lambda\rangle$ and applies the single particle operator an appropriate number of times. From the diagonal basis a transformation to a general basis yields:

$$\hat{O}_1 = \sum_{\mu\nu} \langle \mu|\hat{o}|\nu\rangle a_\mu^\dagger a_\nu. \tag{2.11}$$

To describe pairwise interactions such as Coulomb-interaction or electron-phonon interaction, two body operators need to be introduced. The procedure is somewhat more cumbersome than the single particle operator and the result is simply stated here in a general basis as:

$$\hat{O}_2 = \sum_{\lambda\lambda'\mu\mu'} O_{\mu\mu'\lambda\lambda'} a_\mu^\dagger a_{\mu'}^\dagger a_\lambda a_{\lambda'} \tag{2.12}$$

where $O_{\mu\mu'\lambda\lambda'} = \langle \mu,\mu'|\hat{O}_2|\lambda,\lambda'\rangle$. Although operators for n-body interactions are possible to describe in the second quantization language, they are rarely used in condensed matter physics and are therefore not described here.

2.2 Mean field theory

Describing the dynamics of a many-body system consisting of mutually interacting particles can be a very difficult problem. Only in rare cases, such as the **Ising model** in 1-D or 2-D can the solution be determined exactly.

Although the mutual interactions can be very strong, sometimes a more simplified approach can produce accurate results. Instead of considering the system of mutual interactions, it is possible to view the particles as almost free, and only experiencing the average interaction with the other particles. This procedure reduces the problem from a many-body problem to an effective one particle problem, which is in principle always solvable.

As an example of the mean field approach, consider a system consisting of two kinds of particles, a- and b-types that only interact with the other kind [17]. The second quantization Hamiltonian would then have the following form:

$$H = \sum_\nu \epsilon_\nu^a a_\nu^\dagger a_\mu + \sum_\mu \epsilon_\mu^b b_\mu^\dagger b_\mu + \sum_{\nu\nu'\mu\mu'} V_{\nu\mu\nu'\mu'} a_\nu^\dagger a_{\nu'} b_\mu^\dagger b_{\mu'}. \tag{2.13}$$

The third term, the interaction term, consists of four operators in pairs. This is what makes the problem hard to solve. If it can be assumed that the density operators $a_\nu^\dagger a_{\nu'}$, $b_\mu^\dagger b_{\mu'}$ deviate only little from their expectation value the four-operator terms can be written as:

$$a_\nu^\dagger a_{\nu'} b_\mu^\dagger b_{\mu'} = \Big(\langle a_\nu^\dagger a_{\nu'}\rangle + (a_\nu^\dagger a_{\nu'} - \langle a_\nu^\dagger a_{\nu'}\rangle)\Big)\Big(\langle b_\mu^\dagger b_{\mu'}\rangle + (b_\mu^\dagger b_{\mu'} - \langle b_\mu^\dagger b_{\mu'}\rangle)\Big) \approx$$

$$\langle a_\nu^\dagger a_{\nu'}\rangle b_\mu^\dagger b_{\mu'} + a_\nu^\dagger a_{\nu'}\langle b_\mu^\dagger b_{\mu'}\rangle - \langle a_\nu^\dagger a_{\nu'}\rangle\langle b_\mu^\dagger b_{\mu'}\rangle. \tag{2.14}$$

In the step above, the term where the deviations are multiplied together is considered small and is neglected. With this mean field approach, the Hamiltonian can now be written as:

$$H_{MF} = H_0 + V_{MF} \tag{2.15}$$

where

$$H_0 = \sum_\nu \epsilon_\nu^a a_\nu^\dagger a_\mu + \sum_\mu \epsilon_\mu^b b_\mu^\dagger b_\mu \tag{2.16}$$

and

$$V_{MF} = \sum_{\nu\nu'\mu\mu'} V_{\nu\mu\nu'\mu'}\left[\langle a_\nu^\dagger a_{\nu'}\rangle b_\mu^\dagger b_{\mu'} + a_\nu^\dagger a_{\nu'}\langle b_\mu^\dagger b_{\mu'}\rangle - \langle a_\nu^\dagger a_{\nu'}\rangle\langle b_\mu^\dagger b_{\mu'}\rangle\right]. \tag{2.17}$$

Since the Hamiltonian now is quadratic it can be solved by a unitary transformation. The expectation values have to be solved self-consistently by calculating the averages self consistently:

$$\begin{aligned} \bar{n}^a_{\nu\nu'} &= \langle a_\nu^\dagger a_{\nu'}\rangle, \\ \bar{n}^b_{\mu\mu'} &= \langle b_\mu^\dagger b_{\mu'}\rangle \end{aligned} \tag{2.18}$$

or by minimizing the free energy $F_{MF} = -\frac{1}{\beta}\ln(\mathrm{Tr}\ e^{-\beta H_{MF}})$:

$$\begin{aligned} \langle a_\nu^\dagger a_{\nu'}\rangle: &\quad \frac{\partial F_{MF}}{\partial\langle a_\nu^\dagger a_{\nu'}\rangle} = 0 \\ \langle b_\mu^\dagger b_{\mu'}\rangle: &\quad \frac{\partial F_{MF}}{\partial\langle b_\mu^\dagger b_{\mu'}\rangle} = 0 \end{aligned} \tag{2.19}$$

These two different ways can in fact be shown to be identical [17]. But how is it possible to decide if the mean field theory treatment gives reasonable results? The answer is to use the neglected deviations as perturbations to the theory and check if the result is close to the expectation value. If it is not, the mean field theory either fails or other mean fields have to be chosen.

2.3 Pictures of quantum mechanics

When treating time dependence in quantum mechanics, its useful to distinguish between three different kinds of treatments, so called **pictures**. It is possible to transform between the pictures and they are useful in different contexts. A brief introduction, following [18], to these pictures is given below.

The Schrödinger picture: Here, quantum mechanical operators are considered stationary, $O(0) = O_S(0)$ while the quantum states evolve in time according to the Schrödinger equation, $i\partial_t|\psi(t)\rangle_S = H|\psi(t)\rangle_S$.

The Heisenberg picture: The Heisenberg picture is the opposite to the Schrödinger picture in the sense that quantum states are stationary, $|\psi(t)\rangle = |\psi(0)\rangle_H$ and the operators depend on time according to $O_H(t) = e^{iHt}O_S(0)e^{-iHt}$.

The interaction picture: This picture can be seen as a mixture of the pictures above. For a Hamiltonian on the form $H = H_0 + V_I(t)$, the states evolve with the complicated interaction part V_I according to $|\psi(t)\rangle_I = e^{iH_0t}e^{-iHt}|\psi(0)\rangle_S \Rightarrow i\partial_t|\psi(t)\rangle_I = V_I(t)|\psi(t)\rangle_I$. The operators on the other hand, depend only on the non-interacting part of the Hamiltonian: $O_I(t) = e^{iH_0t}O_S(0)e^{-iH_0t} \Rightarrow i\partial_t O_I(t) = [O_I(t),H_0]$.

In the interaction picture, the quantum state time evolution can be formulated by the introduction of the **time evolution operator**

$$U(t) = e^{iH_0t}e^{-iHt} \tag{2.20}$$

which evolves states from time 0 to t. To evolve from another time than $t = 0$ the operator

$$S(t,t') = U(t)U^\dagger(t') = e^{iH_0(t-t'}e^{-iH(t-t')} \tag{2.21}$$

is defined. This operator can be shown to obey the equation

$$i\partial_t S(t,t') = V_I(t)S(t,t') \tag{2.22}$$

with the solution

$$S(t,t') = T\{\exp(-i\int_{t'}^{t} dt'' V_I(t''))\}, \tag{2.23}$$

where T is the **time ordering operator** which puts operators in order from later times to earlier times. The reason for all this work is that it makes it possible to calculate how a well known system, H_0 changes when $V_I(t)$ is turned on. The key to the solution of this problem is the **Gell-Mann Low theorem** which states that if the interaction is turned on adiabatically (slowly) the H_0 ground state $|\Phi\rangle$ will evolve into the full system ground state $|\Omega\rangle$ according to

$$|\Omega\rangle = S(0,-\infty)|\Phi\rangle, \quad \langle\Omega| = \langle\Phi|S(\infty,0) \tag{2.24}$$

A two point correlation function or **Green's function** (see next section) on the form

$$G(x,x',t,t') = -i\frac{\langle\Phi|T\{\psi_H(x,t)\psi_H^\dagger(x',t')\}|\Phi\rangle}{\langle\Phi|\Phi\rangle} \tag{2.25}$$

will then by interactions evolve into

$$G(x,x',t,t') = -i\frac{\langle\Omega|T\{\psi_H(x,t)\psi_H^\dagger(x',t')\}|\Omega\rangle}{\langle\Omega|\Omega\rangle} =$$

$$-i\frac{\langle\Phi|T\{\psi_H(x,t)\psi_H^\dagger(x',t')\exp(-i\int_{-\infty}^{\infty}dt''V_I(t''))\}|\Phi\rangle}{\{\Phi|T\{\exp(-i\int_{-\infty}^{\infty}dt''V_I(t''))|\Phi\rangle}. \tag{2.26}$$

The S-operator can then be expressed as a Taylor-expansion of the exponential where a desirable amount of the terms can be considered. This is usually the starting point for many perturbative calculations. When doing the expansion it is convenient to express the terms with a diagrammatic representation known as **Feynman diagrams**. Calculations show that diagrams that are not topologically connected cancel by the denominator in the Green's function expression. Hence, calculations can be done by summing connected diagrams. For further reading, consider [19], chapter 4.

2.4 Equilibrium Green's functions

Consider the following differential equation

$$L_x f(x) = \lambda(x), \tag{2.27}$$

where L_x is a linear differential operator, $f(x)$ is the sought function and $\lambda(x)$ is another function. To solve this equation, it is very convenient to assign a so called **Green's function** to the operator L_x with the following definition:

$$L_x G(x) = \delta(x), \tag{2.28}$$

where $\delta(x)$ is the Dirac delta function. If this equation can be solved, the solution to (2.27) can obtained for every $\lambda(x)$ as

$$f(x) = \int G(x - x')\lambda(x')dx' \tag{2.29}$$

since the linearity of L_x assures that

$$L_x f(x) = L_x \int G(x-x')\lambda(x')dx' = \int L_x G(x-x')\lambda(x')dx' = \int \delta(x-x')\lambda(x')dx' = \lambda(x). \tag{2.30}$$

Obtaining the Green's function is usually simpler than solving the differential equation itself which makes the Green's function method very useful.

In the realm of thermal equilibrium many-body quantum mechanics, the use of the word Green's function is slightly different from the description above. Here it is useful to define three Green's functions [20] as:

$$\begin{aligned} G^R(t,t') &= -i\theta(t-t')\langle[A(t),B(t')]_\zeta\rangle \\ G^A(t,t') &= i\theta(t'-t)\langle[A(t),B(t')]_\zeta\rangle \\ G^C(t,t') &= -i\langle T\{A(t)B(t')\}\rangle \end{aligned} \tag{2.31}$$

where $A(t)$ and $B(t')$ are operators in the Heisenberg picture, $\langle ...\rangle$ denotes the average with respect to the ground state by $\langle A\rangle = Z^{-1}\mathrm{Tr}(\rho A)$ and T is the time ordering operator. The Green's functions are in order, the **retarded**, **advanced** and **casual** Green's functions and are most useful at zero temperature. The usefulness of the Green's functions are that they are related to observable quantities such as currents or the **density of states**.

It can be shown that if the Hamiltonian is independent of time, all Green's functions only depend on time differences, i.e. $G(t,t') = G(t-t')$. This can be used to define a Fourier transform for the Green's function in the following way:

$$G^{R,A}(\omega) = \int_\infty^\infty G(t-t')e^{i\omega^\pm(t-t')}d(t-t'). \tag{2.32}$$

where $\omega^\pm = \omega \pm is$, $s \to 0^\pm$ to account for the retarded and advanced Green's function different time domains.

Effects of interaction

When introducing interactions in a theory as described in section 2.3, the Green's function of the full theory, G can be related to the free theory Green's function, G_0, by an equation called the **Dyson equation**:

$$G = G_0 + G_0 \cdot \Sigma \cdot G, \tag{2.33}$$

where the "$\cdot$" denotes a convolution over the used representation variables (for example position and time) and the quantity Σ is called the **self-energy** and encodes the effects of interaction. By the Dyson equation, the task of investigating interactions reduces to finding the self-energy. It can be shown that for a free theory with the following retarded Green's function:

$$G_0^R(k,\omega) = \frac{1}{\omega - \epsilon_k + i\delta}, \tag{2.34}$$

the effect of introducing interactions modifies the Green's function to

$$G^R(k,\omega) = \frac{1}{\omega - \epsilon_k - \Sigma}. \tag{2.35}$$

The number δ is a small, positive and real quantity that is to be taken to zero after calculations. It ensures the analyticity of the Green's functions and is required for convergence in computer calculations. It is not needed here in the full Green's function expression and can be taken to zero immediately. Next, it is useful to introduce a concept called the **spectral function**, which describes how the energy of a particle is distributed over the energy domain. It is defined as

$$A(k,\omega) = -2\mathrm{Im}\left[G^R(k,\omega)\right]. \tag{2.36}$$

For the free electrons, the spectral density can be calculated to be

$$A_0(k,\omega) = -2\mathrm{Im}\left[G_0^R(k,\omega)\right] = -2\delta(\omega - \epsilon_k), \tag{2.37}$$

which is a series of delta peaks distributed over the single particle energies.

By the introduction of interactions by Σ, the spectral function is modified to

$$A(k,\omega) = \frac{2\Gamma}{\sigma^2 + \Gamma^2},\ \sigma = \omega - \epsilon_k - \mathrm{Re}\left[\Sigma\right],\ \Gamma = -\mathrm{Im}\left[\Sigma\right]. \tag{2.38}$$

The density of states can be obtained from the spectral function from the following definition:

$$D(\omega) = \frac{1}{2\pi}\mathrm{Tr}A(k,\omega). \tag{2.39}$$

The interpretation of the density of states is that it is a measure of how many available states there are per energy interval for each energy. It is a quantity that is observable through experiments such as STS, see section 1.4. By comparing the expressions (2.37) and (2.38), it can now be observed that the effect of interactions transforms the delta function into a Lorentzian function. Thereby, the interactions shift the single particle spectrum by the real part of the self-energy and give a broadening, which is interpreted as the particle life time, by the self-energy's imaginary part.

Matsubara Green's functions

In addition to the three Green's functions above it is convenient to define an additional **temperature** or **Matsubara** Green's function as:

$$G(\tau,\tau') = -\langle T_t\{A(-i\tau)B(-i\tau')\}\rangle. \tag{2.40}$$

It has been found to be most useful for computing properties of condensed matter systems at finite temperatures. The Matsubara Green's function is a remarkable entity in the sense that it depends on a **complex time**. Matsubara made the identification that the Boltzmann factor , $exp(\beta H)$, in the density matrix, and the time evolution operator, $exp(-iHt)$ have similar structures [21]. By going to a complex time $t \to -i\tau$ this similarity can be exploited in calculations. A consequence of this so called **Wick rotation** is that inverse temperature is put to equal footing with time.

Performing a Wick rotation and considering a time independent Hamiltonian it can be shown that also the Matsubara Green's function only depends on the difference between the time variables; $G(\tau,\tau') = G(\tau - \tau')$. By similar argumentation as for the zero temperature Green's functions, a Fourier transform may be defined on the form:

$$G(\tau - \tau') = G(\tau) = \frac{1}{\beta}\sum_n \bar{G}(i\omega_n)e^{-i\omega_n\tau} \tag{2.41}$$

where $n \in \mathbb{Z}$ and $\omega_n = 2(n+1)\pi/\beta$ for fermions and $\omega_n = 2n\pi/\beta$ for bosons. These are called the **Matsubara frequencies** and encodes the statistical differences between bosons and fermions.

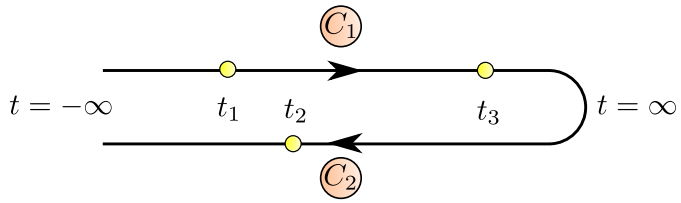

Figure 2.1: *The figure shows the Keldysh time contour consisting of two branches, C_1 and C_2. The contour goes from $t = -\infty$ to $t = \infty$. In this particular configuration $t_1 < t_2 < t_3$ but along the contour $t_1 <_C t_3 <_C t_2$.*

2.5 Non-equilibrium Green's functions

In the above section, equilibrium was considered. When investigating systems in non-equilibrium one wants to know how they change with time. Following [18] again, a time-dependence is introduced by an additional part added to the Hamiltonian by:

$$H = h + H'(t), \tag{2.42}$$

where h is the equilibrium Hamiltonian. The term $H'(t)$ is the time-dependent part which is switched on at time t_0 and is thus breaking the equilibrium. To calculate how a system behaves in non-equilibrium, one usually defines the so called **Contour ordered Green's function**:

$$G(1,1') \equiv -i\langle T_c\{\psi_H(1)\psi_H^\dagger(1')\}\rangle, \tag{2.43}$$

where the notation $(1) = (t_1,\vec{x}_1)$ is used. This Green's function is defined on a complex time contour depicted in figure 2.1.

The time-ordering symbol T_C orders operators according to where t_1 and $t_{1'}$ lies on the contour. Times that appear on the upper part of the contour, C_1 is defined as earlier than times on the lower part, C_2. The contour ordered Green's function can then be seen to contain four different functions depending on where the times are ordered on the contour, see figure 2.2:

$$G(1,1') = \begin{cases} G_c(1,1') & \text{if } t_1,t_{1'} \in C_1 \\ G^>(1,1') & \text{if } t_1 \in C_2, t_{1'} \in C_1 \\ G^<(1,1') & \text{if } t_1 \in C_1, t_{1'} \in C_2 \\ G_{\tilde{c}}(1,1') & \text{if } t_1,t_{1'} \in C_2 \end{cases} \tag{2.44}$$

These Green's functions are defined as:

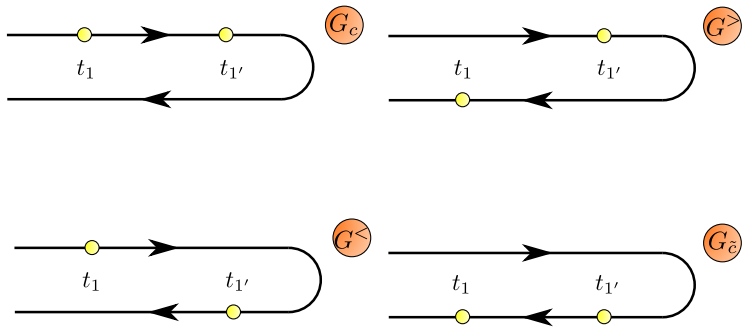

Figure 2.2: *The figure shows the different parts of the contour ordered Green's function. The contour ordered Green's function depends on how the time variables are distributed among the contour branches.*

$$\begin{aligned} G_c(1,1') &= -i\theta(t_1 - t_{1'})\langle\psi_H(1)\psi_H^\dagger(1')\rangle - \zeta i\theta(t_{1'} - t_1)\langle\psi_H^\dagger(1')\psi_H(1)\rangle \\ G^>(1,1') &= -i\langle\psi_H(1)\psi_H^\dagger(1')\rangle \\ G^<(1,1') &= \zeta i\langle\psi_H^\dagger(1')\psi_H(1)\rangle \\ G_{\tilde{c}}(1,1') &= -i\theta(t_{1'} - t_1)\langle\psi_H(1)\psi_H^\dagger(1')\rangle - \zeta i\theta(t_1 - t_{1'})\langle\psi_H^\dagger(1')\psi_H(1)\rangle \end{aligned} \tag{2.45}$$

which in order are the **casual-**, **greater-**, **lesser-** and **anti-casual Green's functions**. In fact, the functions are not independent which can be seen from the fact that $G_c + G_{\tilde{c}} = G^> + G^<$. This means that there are only three independent functions which implies a freedom to choose different conventions. Among these, a popular one is to introduce two new functions, the **retarded** and **advanced** Green's functions:

$$\begin{aligned} G^R(1,1') &= \theta(t_1 - t_{1'})\left[G^>(1,1') - G^<(1,1')\right] \\ G^A(1,1') &= \theta(t_{1'} - t_1)\left[G^<(1,1') - G^>(1,1')\right]. \end{aligned} \tag{2.46}$$

It can be shown that the equilibrium and non-equilibrium treatments of interactions are structurally equivalent and that the difference only lies in replacing ordinary time integrals with integrals on the time contour. For more reading, consider [18, 22, 23].

2.6 Keldysh Formalism

By neglecting any initial correlations it is possible to take care of the contour ordering by the use of 2x2-matrices. This is called the **Keldysh formalism**. There are many ways of doing this but one popular choice order the Green's functions in the following way:

$$G \to \check{G} = \begin{bmatrix} G_c & G^< \\ G^> & G_{\tilde{c}} \end{bmatrix}. \tag{2.47}$$

Here, any variable dependence of the functions have been suppressed for simpler notation. The ordering into this type of matrix has one disadvantage though, and that is that it contains the redundancy from the linear dependence of the functions. To overcome this, it is convenient to make a unitary transformation in this **Keldysh space**, which allows this matrix to be put on a simpler form according to:

$$\check{G} = \begin{bmatrix} G^R & G^K \\ 0 & G^A \end{bmatrix}. \tag{2.48}$$

where G^R and G^A are the retarded and advanced Green's functions and G^K is the **Keldysh Green's function** which has the form

$$G^K(1,1') = G^>(1,1') + G^<(1,1') = -i\langle[\psi_H(1),\psi_H^\dagger(1')]_\zeta\rangle. \tag{2.49}$$

The two different orderings of the functions are connected by the following identities:

$$G^{><} = \frac{1}{2}(G^K) \pm G^R \mp G^A). \tag{2.50}$$

These formulas will be useful in chapter 4.

3

The Kondo lattice

In this chapter we will study a Kondo lattice system. First, we define a model Hamiltonian and introduce the concept of **slave-bosons**. The Hamiltonian is then treated by the mean field scheme which effectively defines a single-electron problem in which the Hamiltonian can be diagonalized in momentum space due to translational invariance. By using Green's functions, the equations governing the behaviour of this system can be derived. The solution to these equations are presented in the results chapter. This chapter is inspired by the work of [10, 11, 24].

3.1 The Hamiltonian and slave-boson construction

Our starting point is the Anderson-Heisenberg Hamiltonian on the form:

$$H = -\sum_{ij\sigma}(t_{ij} + \mu\delta_{ij})c^\dagger_{i\sigma}c_{j\sigma} + \sum_{ij\sigma}\left[V_{ij}c^\dagger_{i\sigma}\tilde{f}_{j\sigma} + H.c.\right] + U\sum_i n^f_{i\uparrow}n^f_{i\downarrow} +$$

$$+\sum_{i\sigma}(\epsilon_f - \mu)\tilde{f}^\dagger_{i\sigma}\tilde{f}_{i\sigma} + \frac{J_H}{2}\sum_{ij}\vec{S}_i \cdot \vec{S}_j. \tag{3.1}$$

The operator $c^\dagger_{i\sigma}$ ($c_{i\sigma}$) creates (annihilates) a conduction electron at site i with spin projection σ and $\tilde{f}^\dagger_{j\sigma}$ ($\tilde{f}_{j\sigma}$) represents similarly a localized f-electron. The hopping amplitude for conduction electrons between sites are denoted as t_{ij}, μ is the chemical potential, ϵ_f is the local energy of the f-orbitals and the hybridization between a conduction electron at site i and a localized f-orbital at site j is represented by V_{ij}. The Coulomb repulsion

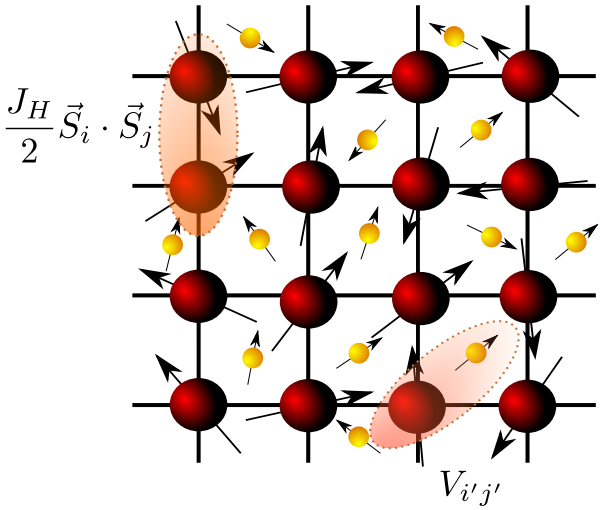

Figure 3.1: *A conceptual picture of the Kondo lattice model on a two-dimensional square lattice. The red balls describe localized magnetic moments placed at the lattice sites, while the yellow balls represent conduction electrons. The magnetic moments interact among themselves with interaction strength J_H and itinerant electrons hybridize with the magnetic moments by the interaction V_{ij}.*

strength for double occupancy in the magnetic moment orbital is given by U and $n^f_{i\sigma}$ is the f-electron number operator for spin projection σ at site i.

The exchange interaction with strength $J_H/2$ between lattice sites is represented by the last term, where the f-electron spins are represented by Abrikosov pseudo-fermions as

$$\vec{S}_i = \frac{1}{2}\sum_{\alpha\beta} \tilde{f}^\dagger_{i\alpha}\vec{\sigma}_{\alpha\beta}\tilde{f}_{i\beta} \tag{3.2}$$

where $\vec{\sigma}$ is the vector of Pauli-matrices. This representation fulfill the $SU(2)$-spin algebra:

$$[S_i,S_j] = i\epsilon^{ijk}S_k. \tag{3.3}$$

where now i,j,k are the spin vector components. By this choice, we have fixed our magnetic moments to be spin 1/2.

In this thesis, we study the case where $U \to \infty$, the so called infinite-U model. This limit excludes any double occupancy in the f-orbitals at every site in the lattice. Algebraically, this limit is enforced by excluding the U-term from the Hamiltonian and instead introducing a slave-boson representation. We then replace the f-electron operator $\tilde{f}_{i\sigma}$ with two auxiliary operators $f_{i\sigma}b^\dagger$, where $f_{i\sigma}$ is a fermionic operator and $b^\dagger$ is

bosonic. The bosons operators work as projectors onto a reduced Hilbert space in the following way:

Consider for simplicity a single site in a conduction electron sea and suppose the system is in the state $|b^1 f^0\rangle$; that is one boson and zero f-electrons present. If the transformed hybridization term operator $f^\dagger_\sigma c_{i\sigma} b$ acts on this state, it will become $|b^0 f^1\rangle$. All other terms in the Hamiltonian either leave the state unaltered or annihilate it. Acting again with the Hamiltonian will by $f^\dagger_\sigma c_{i\sigma} b$ destroy the state $|b^0 f^1\rangle$ but the operator $c^\dagger_{i\sigma} f_\sigma b^\dagger$ brings $|b^1 f^0\rangle$ back again.

If the system is initiated in either $|b^1 f^0\rangle$ or $|b^0 f^1\rangle$ it will never leave this subspace by the slave-boson construction. However, if the system starts in the state $|b^1 f^1\rangle$, a forbidden double occupancy state $|b^0 f^2\rangle$ would be created. To eliminate the possibility of such states we have to employ the following local constraint:

$$b^\dagger_i b_i + \sum_\sigma f^\dagger_{i\sigma} f_{i\sigma} = 1. \tag{3.4}$$

The constraint can be included into the Hamiltonian by a Lagrange multiplier term on the form

$$\sum_i \lambda_i (b^\dagger_i b_i + \sum_\sigma f^\dagger_{i\sigma} f_{i\sigma} - 1). \tag{3.5}$$

With this construction, every site in the Kondo lattice will be singly occupied and therefore have a magnetic moment, cf section 1.2.

3.2 Mean field treatment

Next, we turn our attention to the exchange term. By using the Pauli-matrix identity $\vec{\sigma}_{\alpha\beta} \cdot \vec{\sigma}_{\gamma\delta} = 2\delta_{\alpha\delta}\delta_{\beta\gamma} - \delta_{\alpha\beta}\delta_{\delta\gamma}$, one can show that up to a chemical potential shift (that is terms proportional to the number operator) the exchange term becomes:

$$\vec{S}_i \cdot \vec{S}_j = -\frac{1}{2} \sum_\alpha \tilde{f}^\dagger_{i\alpha} \tilde{f}_{j\alpha} \sum_\beta \tilde{f}^\dagger_{j\beta} \tilde{f}_{i\beta}. \tag{3.6}$$

We now employ the mean field treatment to this four-operator term and by denoting $\chi_{ij} = \frac{J_H}{2} \langle f^\dagger_{i\sigma} f_{j\sigma} \rangle$ we get:

$$\frac{J_H}{2} \sum_{ij} \vec{S}_i \cdot \vec{S}_j \approx -\frac{1}{2} \sum_{ij\sigma} (\chi_{ij} \tilde{f}^\dagger_{j\sigma} \tilde{f}_{i\sigma} + \chi^*_{ij} \tilde{f}^\dagger_{i\sigma} \tilde{f}_{j\sigma}) + \sum_{ij} \frac{|\chi_{ij}|^2}{J_H}. \tag{3.7}$$

The last term is just a total energy term and will not be considered in further calculations.

One further step in the mean field treatment is to assume that the slave bosons are frozen and replaced by their expectation values: $b_i = \langle b_i \rangle = b$ and $b_i^\dagger = \langle b_i^\dagger \rangle = b$. We also assume a site-independent Lagrange multiplier $\lambda_i = \lambda$.

Our total Hamiltonian can now be written as:

$$H = -\sum_{ij\sigma}(t_{ij} + \mu\delta_{ij})c_{i\sigma}^\dagger c_{j\sigma} + b\sum_{ij\sigma}\left[V_{ij}c_{i\sigma}^\dagger f_{j\sigma} + H.c.\right]$$

$$-\sum_{ij\sigma}\left[\chi_{ij} - (\epsilon_f + \lambda - \mu)\delta_{ij}\right] f_{i\sigma}^\dagger f_{j\sigma} + \sum_i \lambda(b^2 - 1). \tag{3.8}$$

The constraints determining the values of the mean fields can be deduced by minimizing the free energy of this Hamiltonian for each parameter θ. By using the Hellmann-Feynman theorem, $\partial\langle H\rangle/\partial\theta = \langle \partial H/\partial\theta\rangle$, taking the expectation value and differentiating with respect to λ and setting this equal to zero, we obtain:

$$N(b^2 - 1) + \sum_{i\sigma}\langle f_{i\sigma}^\dagger f_{i\sigma}\rangle \Leftrightarrow \frac{1}{N}\sum_{i\sigma}\langle f_{i\sigma}^\dagger f_{i\sigma}\rangle + b^2 = 1. \tag{3.9}$$

This is the averaged constraint we initially imposed. Differentiating with respect to b yields the following equation:

$$Nb\lambda + \sum_{j\sigma} V_{ji}\langle c_{j\sigma}^\dagger f_{i\sigma}\rangle = 0. \tag{3.10}$$

The chemical potential μ must be determined such that it gives the desired average electron number per site, ν:

$$\nu = \frac{1}{N}\sum_{i\sigma}\langle c_{i\sigma}^\dagger c_{i\sigma}\rangle + \frac{1}{N}\sum_{i\sigma}\langle f_{i\sigma}^\dagger f_{i\sigma}\rangle \tag{3.11}$$

These averages are most conveniently calculated by using Green's functions. Our next step is to diagonalize the Hamiltonian in momentum space and to calculate the mean field single electron Green's functions.

3.3 Diagonalization and Green's functions

So far, we have said nothing about the actual lattice of the system. In this thesis, we consider a two-dimensional square lattice. The conducting electron hopping between the sites is restricted to nearest neighbour hopping only, i.e. $t_{ij} = t\delta_{i,i+a}$, where a

denotes a nearest neighbour lattice vector. The same restriction is made to the exchange interaction so that only sites that are neighbours interact: $\chi_{ij} = \chi\delta_{ij}$. This means that every site has four nearest neighbours denoted by a_1, a_2, a_3 and a_4. We set the lattice spacing equal to 1 and thus use this as our reference of length. The nearest neighbour vectors are then $\hat{x}$, $-\hat{x}$, $\hat{y}$ and $-\hat{y}$.

The conduction electron part of the Hamiltonian becomes in this nearest neighbour approach:

$$H_{electron} = -t\sum_{i\sigma} c^{\dagger}_{i\sigma}(c_{i+a_1,\sigma} + c_{i+a_2,\sigma} + c_{i+a_3,\sigma} + c_{i+a_4,\sigma}) - \mu\sum_{i\sigma} c^{\dagger}_{i\sigma}c_{i\sigma} \tag{3.12}$$

If we now Fourier-transform the operators into momentum-space by

$$c_{i\sigma} = \frac{1}{\sqrt{N}}\sum_{k} e^{-ix_i\cdot k}c_{k\sigma} \tag{3.13}$$

where N is the number of sites and k denotes a two-dimensional momentum-vector, we get:

$$H_{electron} = -\frac{t}{N}\sum_{kk'\sigma i} c^{\dagger}_{k\sigma}c_{k'\sigma}(e^{ik_x} + e^{-ik_x} + e^{ik_y} + e^{-ik_y}) - \frac{\mu}{N}\sum_{kk'\sigma,i} c^{\dagger}_{k\sigma}c_{k'\sigma}e^{ix_i\cdot(k-k')}$$

$$= \sum_{k\sigma}\epsilon_k c^{\dagger}_{k\sigma}c_{k\sigma}, \tag{3.14}$$

where $\epsilon_k = -2t(\cos(k_x) + \cos(k_y)) - \mu$ is the electron dispersion relation.

Here we have used the identity

$$\sum_{i} e^{ix_i\cdot(k-k')} = N\delta_{kk'} \tag{3.15}$$

in the last step. This identity will be frequently used in the following calculations.

Next, we consider the hybridization-term. Here we assume an on-site electron hybridization only: $V_{ij} = V\delta_{ij}$. The hybridization term can then by the same calculation above be Fourier-transformed and becomes:

$$H_{hybrid} = bV\sum_{k\sigma}(c^{\dagger}_{k\sigma}f_{k\sigma} + h.c.). \tag{3.16}$$

The third term of the Hamiltonian is treated in the same way and yields:

$$H_{exchange} = \sum_{k\sigma} \chi_k f^\dagger_{k\sigma} f_{k\sigma} \tag{3.17}$$

where the f-electrons now have acquired a dispersion on the form $\chi_k = -2\chi(\cos(k_x) + \cos(k_y)) + \epsilon_f + \lambda - \mu$.

By dropping all constant terms generated above, the Hamiltonian has now been brought to a diagonal form:

$$H = \sum_{k\sigma} \left(\epsilon_k c^\dagger_{k\sigma} c_{k\sigma} + bV(c_{k\sigma} f^\dagger_{k\sigma} + f_{k\sigma} c^\dagger_{k\sigma}) + \chi_k f^\dagger_{k\sigma} f_{k\sigma} \right). \tag{3.18}$$

This can more conveniently be written in matrix-form as:

$$H = \sum_{k\sigma} (c^\dagger_{k\sigma},\, f^\dagger_{k\sigma}) \underbrace{\begin{bmatrix} \epsilon_k & bV \\ bV & \chi_k \end{bmatrix}}_{K} \begin{pmatrix} c_{k\sigma} \\ f_{k\sigma} \end{pmatrix} \tag{3.19}$$

where we have denoted the 2x2-matrix above by K. The eigenvalues of the Hamiltonian can now straight forwardly be obtained and we find them to be given by:

$$E^\pm_k = \frac{1}{2}(\epsilon_k + \chi_k \pm \sqrt{(\epsilon_k - \chi_k)^2 + 4b^2V^2}) \tag{3.20}$$

To investigate the dynamics of the Hamiltonian we use the imaginary time, τ, equations of motion for an operator A:

$$\partial_\tau A = [A,H]_- \tag{3.21}$$

Using the commutation relation $[A,BC]_- = A\,[B,C]_\pm - \zeta\,[A,C]_\pm\,B$ (where $\zeta = +1$ for fermions and $\epsilon = -1$ for bosons), the equations of motion lead to the following differential equations for the annihilation operators of the mean field Hamiltonian:

$$\partial_\tau c_{k,\sigma} = \epsilon_k c_{k\sigma} + bV f_{k\sigma} \tag{3.22}$$

$$\partial_\tau f_{k\sigma} = \chi_k f_{k\sigma} + bV c_{k\sigma} \tag{3.23}$$

The equations of motion for the creation operators can be obtained simply by complex conjugation.

To proceed, we recast the operators in a two component spinor representation:

$$\Psi^\dagger_{k\sigma} = (c^\dagger_{k\sigma}, f^\dagger_{k\sigma}) \ , \quad \Psi_{k\sigma} = \begin{pmatrix} c_{k\sigma} \\ f_{k\sigma} \end{pmatrix} \tag{3.24}$$

Then we can combine the equations of motions for the operators as a matrix equation:

$$\partial_\tau \Psi_{k\sigma} = \begin{bmatrix} \epsilon_k & bV \\ bV & \chi_k \end{bmatrix} \Psi_{k\sigma} \equiv K \Psi_{k\sigma} \tag{3.25}$$

Next, we define the temperature Green's function as follows:

$$G(\mathbf{k},\tau,\sigma) = -\langle T_\tau \Psi_{k\sigma}(\tau) \Psi^\dagger_{k\sigma}(0) \rangle = \ - \langle T_\tau \begin{pmatrix} c_{k\sigma} \\ f_{k\sigma} \end{pmatrix} (c^\dagger_{k\sigma}, f^\dagger_{k\sigma}) \rangle$$

$$= - \begin{bmatrix} \langle T_\tau c_{k\sigma}(\tau) c^\dagger_{k\sigma}(0) \rangle & \langle T_\tau c_{k\sigma}(\tau) f^\dagger_{k\sigma}(0) \rangle \\ \langle T_\tau f_{k\sigma}(\tau) c^\dagger_{k\sigma}(0) \rangle & \langle T_\tau f_{k\sigma}(\tau) f^\dagger_{k\sigma}(0) \rangle \end{bmatrix} \tag{3.26}$$

where T_τ is the imaginary time ordering operator. The differential equation satisfied by this Green's function can be shown to be:

$$(-\partial_\tau - K) G(k,\tau,\sigma) = \delta(\tau)$$

which can be solved by Fourier transformation into Matsubara space:

$$G(k,\tau,\sigma) = \frac{1}{\beta} \sum_{\omega_n} e^{-i\omega_n \tau} \bar{G}(k,\omega_n,\sigma)$$

where $\dfrac{1}{\beta} = k_B T$ is the inverse thermal energy and $\omega_n = (2n+1)\dfrac{\pi}{\beta}$, where $n \in \mathbb{Z}$, are the fermionic Matsubara frequencies. The differential equation transforms into an algebraic one:

$$(i\omega_n - K) \bar{G}(k,\omega_n,\sigma) = 1 \tag{3.27}$$

or more explicitly:

$$\begin{bmatrix} i\omega_n - \epsilon_k & -bV \\ -bV & i\omega_n - \chi_k \end{bmatrix} \begin{bmatrix} \bar{G}_{cc}(k,\omega_n,\sigma) & \bar{G}_{cf}(k,\omega_n,\sigma) \\ \bar{G}_{fc}(k,\omega_n,\sigma) & \bar{G}_{ff}(k,\omega_n,\sigma) \end{bmatrix} = 1 \tag{3.28}$$

The constraints determined in section 3.2 can after a Fourier-transform be expressed in terms of the Green's functions:

$$\begin{cases} \lambda b + V\dfrac{1}{N}\sum_{k\sigma\omega_n} \bar{G}_{cf}(k,\omega_n,\sigma) & = 0 \\ 1 - b^2 - \dfrac{1}{N}\sum_{k\sigma\omega_n} \bar{G}_{ff}(k,\omega_n,\sigma) & = 0 \\ \nu - \dfrac{1}{N}\sum_{k\sigma\omega_n} \bar{G}_{cc}(k,\omega_n,\sigma) - \dfrac{1}{N}\sum_{k\sigma\omega_n} \bar{G}_{ff}(k,\omega_n,\sigma) & = 0 \end{cases} \tag{3.29}$$

These are the equations we are going to solve to investigate the model. The input parameters are the hopping amplitude t, the hybridization strength V, the spin liquid parameter χ, the temperature T, the f-orbital local energy ϵ_f and the filling factor ν. The output values acquired are the Lagrange multiplier λ, the average slave boson field b and the chemical potential μ.

4

Tunneling into the Kondo lattice

In this chapter a simple model of the Kondo lattice in close vicinity to a tunneling microscope is considered. The tip is considered to be of a simple metal material such as the density of states can be approximated as constant. With the use of non-equilibrium Green's functions, a formula for the tunneling current and the differential conductance can be derived. All results are presented in chapter 5.

4.1 Derivation of the tunneling current and conductance

We begin by considering a joint system consisting of the Kondo lattice described in the previous chapter, a metal tip representing the microscope and a possibility of tunneling between the tip and the Kondo lattice. See figure 4.1. This system is modelled by the following Hamiltonian:

$$H = H_{KL} + H_{tip} + H_{tunnel} \tag{4.1}$$

where

$$H_{KL} = \sum_{k\sigma} \left(\epsilon_{k\sigma} c^\dagger_{k\sigma} c_{k\sigma} + bV(c_{k\sigma} f^\dagger_{k\sigma} + f_{k\sigma} c^\dagger_{k\sigma}) + \chi_{k\sigma} f^\dagger_{k\sigma} f_{k\sigma} \right), \tag{4.2}$$

is the Kondo lattice Hamiltonian,

$$H_{tip} = \sum_{k\sigma} \tilde{\epsilon}_{k\sigma} e^\dagger_{k\sigma} e_{k\sigma} \tag{4.3}$$

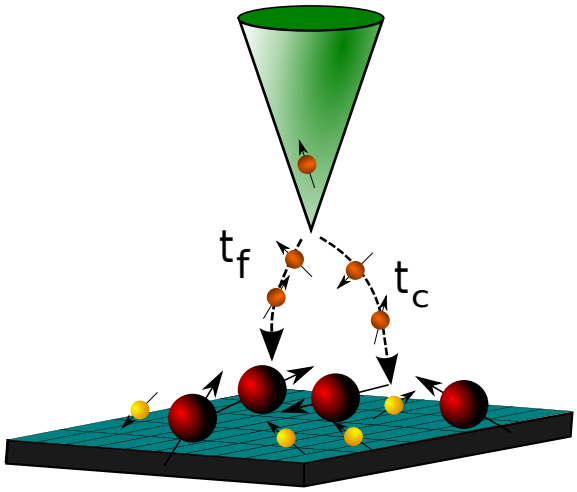

Figure 4.1: *The figure shows a simple description of a tunneling experiment. Electrons from the tip (represented by orange balls) can tunnel into the localized f-electron states, red balls, or itinerant electron states, yellow balls. This allows for two separate tunneling paths with amplitudes, t_f and t_c respectively, and one path where electrons tunnel in a superposition of the two separate paths.*

is the tip Hamiltonian and

$$H_{tunnel} = \sum_{k\sigma} \left[t_c c^\dagger_{k\sigma} e_{k\sigma} + t_f f^\dagger_{k\sigma} e_{k\sigma} + H.c. \right] \tag{4.4}$$

describes the coupling between tip electrons and the states in the Kondo lattice. The amplitudes of tunneling into conduction electron states and localized f-states are denoted as t_c and t_f respectively.

Quantum mechanically, the tunneling current, $I(t,t')$ is given by the change in particle number of the tip times the electric charge. The time derivative is given by the Heisenberg equation of motion which gives the following expression for the current:

$$I(t,t') = -e\langle \dot{N_{tip}} \rangle = -\frac{ie}{\hbar}\langle [H,N_{tip}] \rangle = -\frac{ie}{\hbar}\langle [H_{tip},N_{tip}] \rangle \tag{4.5}$$

since N_{tip} commutes with the other parts of the Hamiltonian. Performing the commutator gives:

$$I(t,t') = \frac{ie}{\hbar} \sum_{k\sigma} \left[t_c \langle e^\dagger_{k\sigma}(t) c_{k\sigma}(t') \rangle + t_f \langle e^\dagger_{k\sigma}(t) f_{k\sigma} \rangle (t') - H.c. \right] =$$

$$\frac{e}{\hbar}\sum_{k\sigma}\left[t_c G^<_{tc}(k,\sigma,t,t') + t_f G^<_{tf}(k,\sigma,t,t') - t_c^* G^{<*}_{ct}(k,\sigma,t,t') - t_f^* G^{<*}_{ft}(k,\sigma,t,t')\right] =$$

$$\frac{2e}{\hbar}\sum_{k\sigma}\mathrm{Re}\left[t_c G^<_{tc}(k,\sigma,t,t')) + t_f G^<_{tf}(k,\sigma,t,t')\right] \tag{4.6}$$

where the definition of the lesser Green's functions have been used together with the fact that $G^<_{ij} = -G^{<*}_{ji}$. To proceed, we consider a steady state current, that is $t = t' = 0$, and we can perform a Fourier transform into the energy domain. The current is then given by:

$$I(0) = I = \frac{2e}{\hbar}\sum_{k\sigma}\int\frac{d\omega}{2\pi}\mathrm{Re}\left[t_c G^<_{tc}(k,\sigma,\omega) + t_f G^<_{tf}(k,\sigma,\omega)\right] \tag{4.7}$$

The task of calculating the current and conductance is now reduced to calculating two lesser Green's functions. Since the current is a non-equilibrium process due to the potential difference between the tip and the Kondo lattice, a Keldysh approach can be used to calculate the non-equilibrium Green's functions. We start with the Dyson equation in the joint system space:

$$G = G_0 + G_0 \cdot T \cdot G \tag{4.8}$$

where "$\cdot$" denotes a convolution in real time. The matrices are the full and equilibrium Green's functions ordered as:

$$G = \begin{bmatrix} \check{G}_{tt} & \check{G}_{tc} & \check{G}_{tf} \\ \check{G}_{ct} & \check{G}_{cc} & \check{G}_{cf} \\ \check{G}_{ft} & \check{G}_{fc} & \check{G}_{ff} \end{bmatrix},\ G_0 = \begin{bmatrix} \check{g}_{tt} & 0 & 0 \\ 0 & \check{g}_{cc} & \check{g}_{cf} \\ 0 & \check{g}_{fc} & \check{g}_{ff} \end{bmatrix},\ T = \begin{bmatrix} 0 & \check{T}_{tc} & \check{T}_{tf} \\ \check{T}_{ct} & 0 & 0 \\ \check{T}_{ft} & 0 & 0 \end{bmatrix} \tag{4.9}$$

and where the "*check*" symbol denotes a Keldysh matrix on the form

$$\check{g} = \begin{bmatrix} g^R & g^K \\ 0 & g^A \end{bmatrix}. \tag{4.10}$$

With this construction, the tunneling amplitude terms $\check{T}_{ij}$, are diagonal in Keldysh space:

$$\check{T}_{tc} = \mathbb{1}_{2x2} t_c. \tag{4.11}$$

The Dyson equation connects the sought non-equilibrium Green's functions to the equilibrium ones, which are known from the previous chapters. The Green's functions we are looking for are $\check{g}_{tc}$ and $\check{g}_{tf}$. By calculating these, we can obtain the lesser Green's functions from the following identity:

$$G^{<}_{ij} = \frac{1}{2}(G^{K}_{ij} - G^{R}_{ij} + G^{A}_{ij}). \tag{4.12}$$

For a steady state and translationally invariant system, the Dyson equation is purely algebraic and can be solved by pure algebraic means. Solving for the lesser Green's functions gives the following final result for the current:

$$I = \frac{4e}{\hbar}\int \frac{d\omega}{2\pi}\left[(t_c^2 D_{cc}(\omega) + 2t_c t_f D_{cf}(\omega) + t_f^2 D_{ff}(\omega))D_{tt}(\omega)(f_{tip}(\omega + eV) - f_{KL}(\omega))\right] \tag{4.13}$$

Here, we have neglected terms of order $t^4_{c/f}$ and used the fact that $G^R_{ij} - G^A_{ij} = -2iD_{ij}$, where D_{ij} is the density of states corresponding to conduction electrons and f-electrons. The term D_{fc} is a quantity similar to a density of states, but it contains terms of the type $\langle c^\dagger f\rangle$ and is related to the hybridization. As will be seen in chapter 5, this term represents interference in the tunneling process which produces a very significant appearance of the differential conductance. The function $f(\omega)$ denotes the Fermi distribution function.

The differential conductance is defined as $G(V) = dI/dV$. It is obtained by straightforward differentiation of equation 4.13.

5

Results and conclusions

In this chapter the results of the two previous chapters are presented. First, the Kondo lattice model from chapter 3 is considered. The solutions to equations 3.29 are presented by calculations of the excitation spectra, hybridization dependence, temperature dependence and the density of states.

Secondly, the tunneling current and differential conductance from chapter 4 is calculated for some specific Kondo lattice parameters. In addition, the differential conductance dependence on the tunneling parameters t_c and t_f is investigated for a simple configuration.

The energy scale is defined by the Kondo lattice conduction electron hopping amplitude by setting $t = 1$ in all calculations. Temperature, frequency and energy are all measured in the same units by setting $k_B = \hbar = 1$.

5.1 The Kondo lattice model

The main results for the Kondo lattice model are the solutions to the equations 3.29. From them, the mean field parameters λ, b and μ can be calculated. These are obtained as a function of input parameters χ, T, e_f, ν, which in order are: the spin-liquid parameter, the temperature, the energy levels of the localized states and the filling factor. A summary of all parameters is presented for reference in table 5.1.

To solve the mean field equations, a multidimensional Newton method has been used. Since the system has translational symmetry, to solve for a single site is sufficient and integrations over the first Brillouin-zone are transformed into sums on the form $\frac{1}{N}\sum_k$ in the computer calculations. Here, $N \sim 500$ is the number of sampling-points used

Table 5.1: *The table shows the various input and output parameters of the Kondo lattice model.*

Parameter	Description	Output/Input
t	Conduction electron hopping amplitude	Input
χ	Spin liquid parameter	Input
T	Temperature	Input
e_f	Local moment energy level	Input
ν	Filling factor	Input
λ	Lagrange multiplier	Output
b	Slave boson mean field	Output
μ	Chemical potential (Fermi level)	Output

in k-space. No significant changes in calculations for different N of this order have been observed. The low N is also chosen with computation time in consideration. All calculations have been done in MATLAB, Java and Fortran 90.

The complex part of the Green's function energy variable, denoted by δ (see section 2.4), can not be taken to zero in computer calculations. Instead, it must be chosen sufficiently small so that divergent peaks are made finite and distinguishable. This choice may be different for different calculations. As a consequence, scales in the density of states and differential conductance are arbitrary, and in this thesis, it is the qualitative features that are important and not specific values.

Excitation spectra

In the following we consider the excitation spectra for k_x only and therefore set $k_y = \pi/2$ which removes all $\cos(k_y)$-terms in the dispersion relations. This gives two-dimensional graphs to study instead of three-dimensional which makes the qualitative features easier to visualize.

Equation 3.20 describes the quasiparticle excitation spectrum as two bands separated with a gap of size $\sqrt{(e_f + \lambda)^2 + 4b^2V^2)}$ at $k_x = \pi/2$. In figure 5.1, the bands in the k_x-direction are plotted together with the conduction electron dispersion, the local moment dispersion and the chemical potential. The range $k_x \in [0,\pi]$ is chosen since the spectrum in the chosen direction is symmetric around $k_x = 0$ and has a period of 2π.

The behaviour of the quasiparticles is for small k_x very similar to f-electrons while for k_x close to π, the Brillouin-zone edge, the behaviour is c-electron- like. However, in the mid section of the k_x-range, it can be observed that the quasiparticles consists of a mixture of c- and f-electrons.

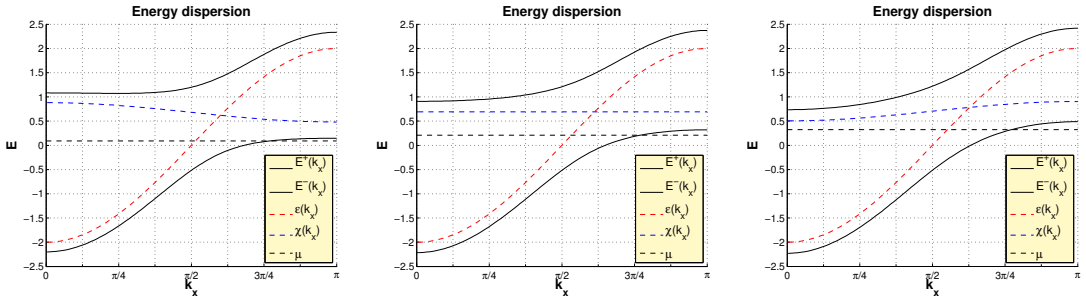

(a) (b) (c)

Figure 5.1: *The figure shows, in the k_x-direction for $k_y = 0$, the excitation spectrum of a two-dimensional square lattice mean field Kondo lattice model. The top filled black line is the quasiparticle top band dispersion $E^+(k_x)$, while the lower filled black line is the lower quasiparticle band dispersion $E^-(k_x)$. The f-dispersion is represented by the blue striped line and the c-dispersion by the red striped line. The chemical potential is the black striped line. The parameters chosen are $V = 1.0$, $T = 0.01$, $ef = 0$ and $\nu = 1.5$ for all three plots and $\chi = -0.1,\ 0.0, 0.1$ for the figures a, b, c respectively. The mean field parameters obtained are for a: $\lambda = 0.68$, $b = 0.79$, $\mu = 0.09$. For b: $\lambda = 0.69$, $b = 0.79$, $\mu = 0.21$ and for c: $\lambda = 0.70$, $b = 0.79$, $\mu = 0.32$.*

From the dispersion-relations, it is possible to calculate the mass-enhancement from formation of these quasiparticles. This is however not done in this thesis. See [3] for further reading. The mass-enhancement can be observed in various experiments such as [3]:

- Renormalization of the Sommerfeld specific heat coefficient $\gamma \to \sim \frac{m*}{m}\gamma$.
- Renormalization of the Pauli susceptibility $\chi_{pauli} \to \sim \frac{m*}{m}\chi_{pauli}$.
- A separation of the Drude optical conductance spectrum into two components separated by a gap. The relaxation rate is also enhanced by the formation of the heavy electrons.

Hybridization strength dependence

In this section, we investigate how the the slave boson field and effective f-site energy depends on the hybridization V. The results are presented in figures 5.2, 5.3 and 5.4. The filling factor is kept constant in contrast to [24] which fixes the chemical potential at $\mu = 0$ and lets the filling adapt differently to every configuration. With our calculations, the filling may instead be chosen, in order to more easily model a simple material. However, the qualitative features of [24] are reproduced in our model.

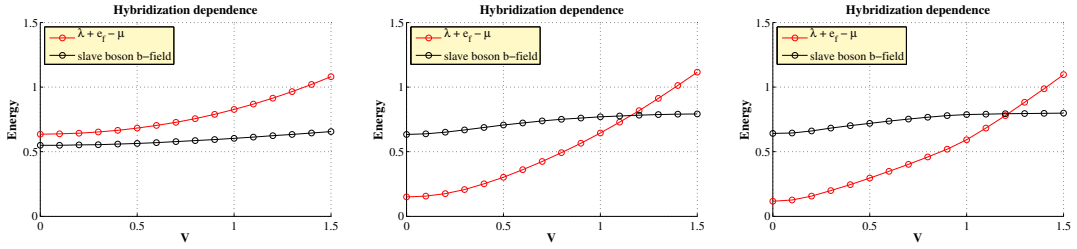

(a) (b) (c)

Figure 5.2: *The figure shows the effective f-electron energy (red dotted line) and the slave boson field (black dotted line) as a function of the hybridization V. The fixed parameters are $\chi = -0.1$, $ef = 0$ and $\nu = 1.5$ for all three plots and $T = 1$, $T = 0.1$ and $T = 0.01$ for the figures a, b, c respectively.*

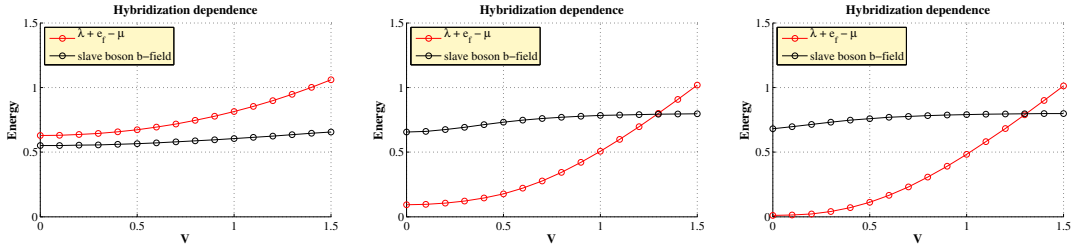

(a) (b) (c)

Figure 5.3: *The figure shows the effective f-electron energy (red dotted line) and the slave boson field (black dotted line) as a function of the hybridization V. The fixed parameters are $\chi = 0.0$, $ef = 0$ and $\nu = 1.5$ for all three plots and $T = 1$, $T = 0.1$ and $T = 0.01$ for the figures a, b, c respectively.*

Our model gives that both the effective f-electron energy, $\lambda + e_f - \mu$ and the slave boson field, b, decreases with lower hybridization strength, V.

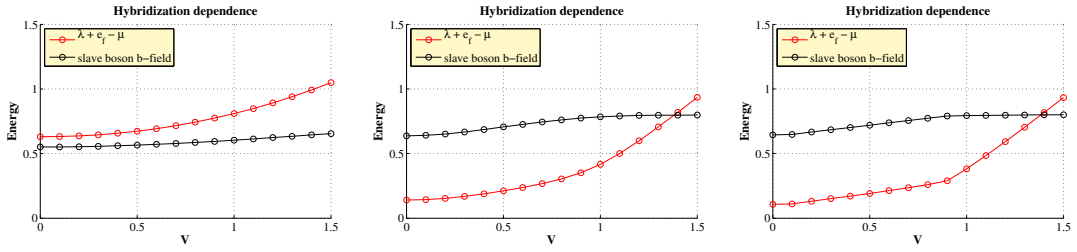

Figure 5.4: *The figure shows the effective f-electron energy (red dotted line) and the slave boson field (black dotted line) as a function of the hybridization V. The fixed parameters are $\chi = 0.1$, $ef = 0$ and $\nu = 1.5$ for all three plots and $T = 1$, $T = 0.1$ and $T = 0.01$ for the figures a, b, c respectively.*

Temperature dependence

The temperature dependence of the mean field parameters is presented in this section. For the fixed parameters, we have chosen the following configuration: $V = 1.0$, $\chi = 0.0$, $e_f = 0.2$ and $\nu = 1.5$.

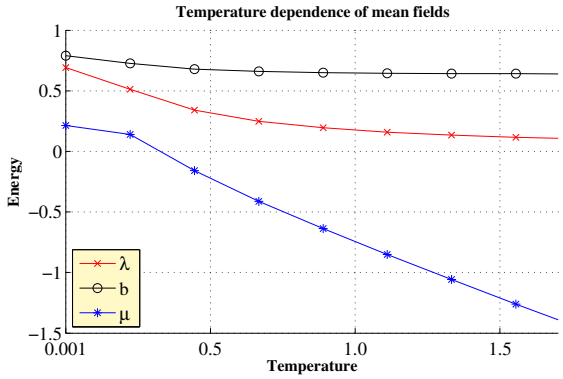

Figure 5.5: *For the $t = 1.0$, $V = 1.0$, $\chi = 0.0$, $e_f = 0.0$ and $\nu = 1.5$, the values of λ, b and μ are plotted as a function of temperature.*

The parameters are seen to not change very much in this temperature range, but to investigate lower temperatures, a more efficient solution method must be developed to decrease the computation time. As can be seen in 3.29, the calculations require infinite summations over Matsubara frequencies which must truncated in computer calculations. In this thesis, the truncation limit is set to $100/T$. This means the lower the temperature, the more frequencies to sum over. To be able to do computations for lower temperatures, a more efficient programming method must be utilized.

Density of states

The density of states can be obtained from the Matsubara Green's function according to:

$$D(\epsilon) = -\frac{1}{\pi} \lim_{\delta \to 0} \mathrm{Im}\,[\ \mathrm{Tr}\ G(i\omega_n, k,\sigma)|_{i\omega_n \to \epsilon + i\delta}] \tag{5.1}$$

where δ denotes a very small number, Im denotes the imaginary part and Tr is the trace which represents in our diagonal momentum and spin representation a summation over k and σ. $G(i\omega_n, k,\sigma)$ is the Matsubara Green function in momentum space.

For three different configurations of our Kondo lattice model, the density of states is plotted in figure 5.6. The most significant feature is the formation of a hybridization gap for $\chi = 0.0$ and $\chi = -0.1$. The density of states calculations reproduce similar results to [24].

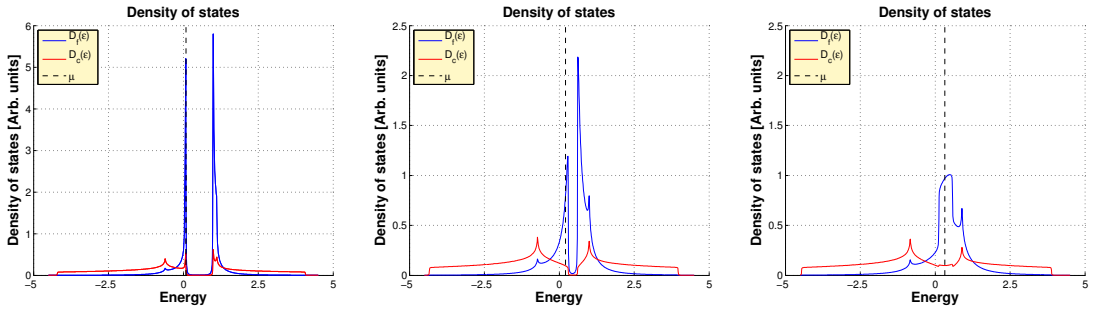

(a) (b) (c)

Figure 5.6: *The figures show the conduction electron (in black) and the f-electron density of states for three different setups of the two-dimensional square Kondo lattice model. The parameters chosen are* $V = 1.0$, $T = 0.01$, $ef = 0$ *and* $\nu = 1.5$ *for all three plots and* $\chi = -0.1, 0.0, 0.1$ *for the figures a, b, c respectively. A value of* $\delta = 0.005$ *has been used for all three figures.*

5.2 Tunneling into the Kondo lattice

In this section, the results of the tunneling setup described in chapter 4 are presented. To obtain the tunneling current and conductance for the Kondo Lattice - tunneling tip system, some approximations have been made. First and most importantly, the tunneling amplitudes are considered to be real and energy independent. Secondly, the tip density of states, $D_{tt}(\omega)$, is assumed to be constant (this is what is sought when designing good tunneling tips) and is set equal to 1 for simplicity. This approximation is equivalent to setting the tip Green's functions to:

$$g_{tt}^{R/A} = \mp i D_{tt} = \mp i \tag{5.2}$$

Further, the voltage difference between the sample and the tip is denoted by V where V is measured in units of energy by setting the electric charge $e = 1$.

Tunneling current and differential conductance

The tunneling current and differential conductance have been calculated for three different setups of the Kondo lattice, and for three different temperatures for each setup. The results are presented in figures 5.8, 5.9 and 5.7. From these figures, it is evident that the typical Fano-shape emerges. This is a phenomena that arises from interference of the tunneling paths and is consistent with [25–27].

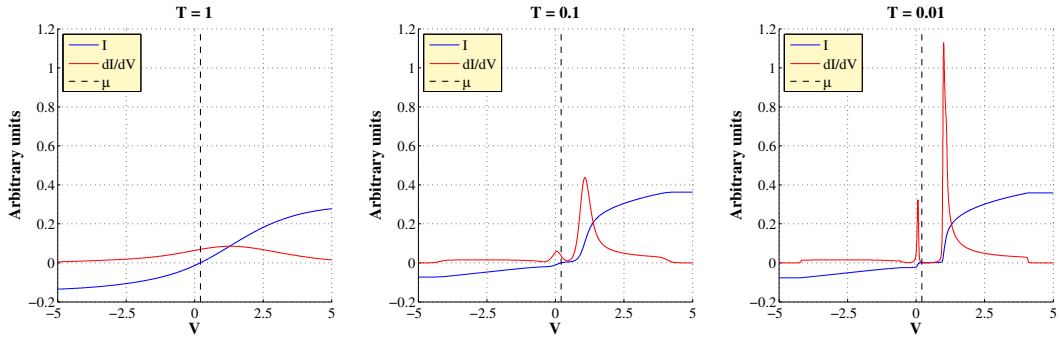

Figure 5.7: *The figure shows the current (blue line) and differential conductance (red line) for a two-dimensional square Kondo lattice. The parameters chosen are* $V = 1.0$, $\chi = -0.1$, $e_f = 0$ *and* $\nu = 1.5$. *The temperature is* $T = 1$, $T = 0.1$ *and* $T = 0.01$ *in order from left to right. The tunneling parameters have been set to* $t_c = t_f = 0.1$.

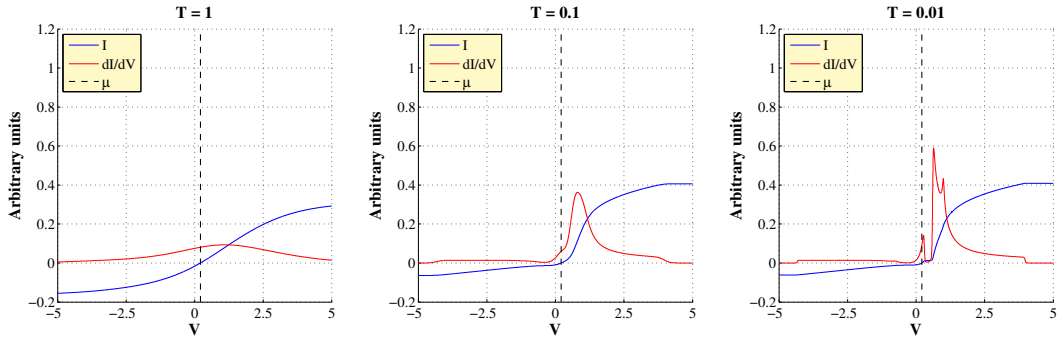

Figure 5.8: *The figure shows the current (blue line) and differential conductance (red line) for a two-dimensional square Kondo lattice. The parameters chosen are* $V = 1.0$, $\chi = 0.0$, $e_f = 0$ *and* $\nu = 1.5$. *The temperature is* $T = 1$, $T = 0.1$ *and* $T = 0.01$ *in order from left to right. The tunneling parameters have been set to* $t_c = t_f = 0.1$.

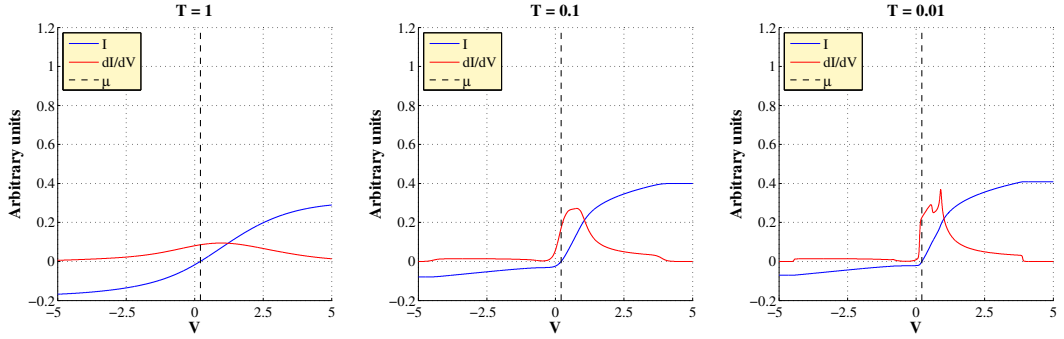

Figure 5.9: *The figure shows the current (blue line) and differential conductance (red line) for a two-dimensional square Kondo lattice. The parameters chosen are* $V = 1.0$, $\chi = 0.1$, $e_f = 0$ *and* $\nu = 1.5$. *The temperature is* $T = 1$, $T = 0.1$ *and* $T = 0.01$ *in order from left to right. The tunneling parameters have been set to* $t_c = t_f = 0.1$.

Tunneling amplitude dependence

The dependence of the tunneling parameters t_c and t_f is depicted in figures 5.10 and 5.11 for the case of $\chi = 0.0$. Notice that when one of the tunneling amplitudes are set to zero, the differential conductance reproduces the density of states for the non-zero tunneling path, compare with figure 5.6(b). This is due to the constant tip density of states approximation, equation 5.2, which agrees good with the STS-description in chapter 1.

In a real STS experiment, the amplitude for tunneling into the conduction band would be larger than the f-states, due to the latter's highly localized nature.

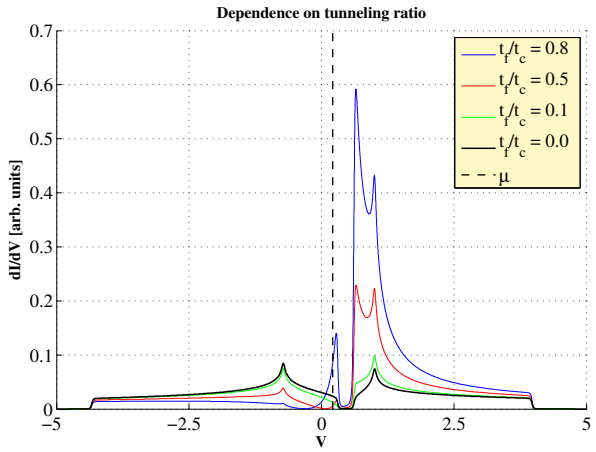

Figure 5.10: *The figure shows the differential conductance as function of the voltage V and the tunneling ratio t_c/t_f for $t_c = 0.1$. The parameters chosen are $V = 1.0$, $\chi = 0.0$, $e_f = 0$, $T = 0.01$ and $\nu = 1.5$.*

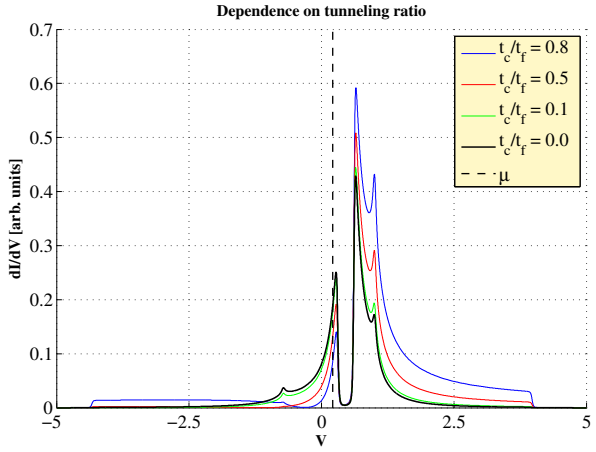

Figure 5.11: *The figure shows the differential conductance as function of the voltage V and the tunneling ratio t_f/t_c for $t_f = 0.1$. The parameters chosen are $V = 1.0$, $\chi = 0.0$, $e_f = 0$, $T = 0.01$ and $\nu = 1.5$.*

6

Summary and outlook

The Kondo lattice model is thought to be a good candidate for describing heavy fermion behaviour. In this thesis, the purpose has been to study a simple version of this model which consists of itinerant electrons hybridizing with localized electrons. The localized electrons constitute a square two-dimensional lattice and interact with their nearest neighbours. This Kondo lattice model has been treated with a mean field slave boson approach and solved self-consistently with Green's functions. The model is found to exhibit a two-band quasiparticle dispersion separated by a gap that depends on the hybridization strength. This gap is also manifested in the density of states.

Further, a system where the Kondo lattice is in close proximity to a tunneling tip has been considered. By employing the Keldysh formalism machinery, a non-equilibrium tunneling current and differential conductance has been calculated. The tunneling setup is seen to give rise to a Fano-lineshape structure of the conductance. In addition, the conductance calculations can, in a single path tunneling configuration, be seen to map out the density of states.

To expand the presented Kondo lattice model, many assumptions can be withdrawn and a more thorough treatment can be made. For example, the mean field approach is usually a very first approximation and attempts to abandon the mean field treatment will probably give more accurate results to be compared with experiments. Further, all Lagrange multipliers and the slave boson field are considered as site-independent which is a crude approximation and can be abandoned for further progress.

In addition, this model only treats a lattice consisting of spin-1/2. Since this is not at all true for most materials of the heavy fermion type, a more general spin-N approach is required for investigating more complicated systems. This is usually done with the so

called large N-expansion which would be interesting to employ to the model considered here.

Another interesting approach to this Kondo lattice model would be to include a superconducting pairing term to the Hamiltonian. This might reveal additional properties which would be exciting to explore. It would also be interesting to calculate the enhancement of the mass of the formed quasiparticles.

Regarding the tunneling calculations, some of the assumptions made, such as constant density of states and constant tunneling amplitudes may be relaxed to improve the accuracy of the results. Other tunneling channels and background noise and background conductance could be added to the system for a more realistic model of a tunneling process.

Generally, it would be interesting to explore the parameter ranges more thoroughly than done in this thesis, and for this reason a more efficient scheme for setting up computer computations would be beneficial.

As a final and perhaps most important point, it is interesting to compare results of the model, both in its present state and by including some of the proposals above, with some experiments. Some general features though, such as the Fano-lineshape is definitely seen in tunneling experiments on the heavy fermion compound URu_2Si_2 [27].

Bibliography

[1] P. Anderson, More is different, Science 177 (4047) (1972) 393–396.
URL http://www.sciencemag.org/content/177/4047/393

[2] P. Davies, God and the New Physics, Pocket Books, 1984.

[3] P. Coleman, Introduction to Many Body Physics, Unpublished, 2012.
URL http://www.physics.rutgers.edu/~coleman/620/mbody/pdf/bkx.pdf

[4] K. Andres, J. Graebner, H. Ott, 4f-virtual-bound-state formation in $CeAl_3$ at low temperatures, Physical Review Letters 35 (26) (1975) 1779–1782.
URL http://link.aps.org/doi/10.1103/PhysRevLett.43.1892

[5] F. Steglich, J. Aarts, C. Bredl, W. Lieke, D. Meschede, W. Franz, H. Schäfer, Superconductivity in the presence of strong Pauli paramagnetism: $CeCu_2Si_2$, Physical Review Letters 43 (25) (1979) 1892–1896.
URL http://link.aps.org/doi/10.1103/PhysRevLett.43.1892

[6] J. Bednorz, K. Müller, Possible high T_c superconductivity in the Ba-La-Cu-O system, Zeitschrift für Physik B Condensed Matter 64 (2) (1986) 189–193.
URL http://dx.doi.org/10.1007/BF01303701

[7] B. Coqblin, M. Nunez-Regueiro, A. Theumann, J. Iglesias, S. Magalhaes, Theory of the kondo lattice: competition between kondo effect and magnetic order, Philosophical Magazine 86 (17-18) (2006) 2567–2580.
URL http://www.tandfonline.com/doi/abs/10.1080/14786430500229349

[8] P. Coleman, Heavy fermions: electrons at the edge of magnetism, Handbook of Magnetism and Advanced Magnetic Materials.
URL http://boulder.research.yale.edu/Boulder-2008/ReadingMaterial-2008/Coleman/coleman_wiley.pdf

[9] H. v. Löhneysen, T. Pietrus, G. Portisch, H. G. Schlager, A. Schröder, M. Sieck, T. Trappmann, Non-fermi-liquid behavior in a heavy-fermion alloy at a magnetic

instability, Physical Review Letters 72 (1994) 3262–3265.
URL http://link.aps.org/doi/10.1103/PhysRevLett.72.3262

[10] D. Newns, N. Read, Mean-field theory of intermediate valence/heavy fermion systems, Advances in Physics 36 (6) (1987) 799–849.
URL http://www.tandfonline.com/doi/abs/10.1080/00018738700101082

[11] A. Hewson, The Kondo Problem to Heavy Fermions, Cambridge Universiy Press, 1997.

[12] P. Phillips, Advanced Solid State Physics, Westview Press, 2003.

[13] J. Kondo, Resistance minimum in dilute magnetic alloys, Progress of Theoretical Physics 32 (1) (1964) 37–49.
URL http://ptp.ipap.jp/link?PTP/32/37/

[14] K. G. Wilson, The renormalization group: Critical phenomena and the kondo problem, Reviews of Modern Physics 47 (1975) 773–840.
URL http://link.aps.org/doi/10.1103/RevModPhys.47.773

[15] J. Stroscio, Scanning Tunneling Microscopy, Academic Press, 1993.

[16] A. Altland, B. Simons, Condensed Matter Field Theory, Cambridge University Press, 2010.

[17] H. Bruus, K. Flensberg, Many-body Quantum Theory In Condensed Matter Physics: An Introduction, Oxford University Press, 2004.

[18] H. Haug, A. Jauho, Quantum Kinetics in Transport and Optics of Semiconductors, Vol. 6, Springer Verlag, 2008.

[19] M. Peskin, D. Schroeder, An Introduction to Quantum Field Theory, Westview Press, 1995.

[20] G. Rickayzen, Green's functions and Condensed Matter, Academic Press, 1980.

[21] T. Matsubara, A new approach to quantum-statistical mechanics, Progress in Theoretical Physics 14 (1955) 351–378.
URL http://ptp.ipap.jp/link?PTP/14/351/

[22] J. Rammer, H. Smith, Quantum field-theoretical methods in transport theory of metals, Reviews of Modern Physics 58 (1986) 323–359.
URL http://link.aps.org/doi/10.1103/RevModPhys.58.323

[23] J. Viljas, On the calculation of green's functions in nonequilibrium fermi systems, Personal notes.
URL http://ltl.tkk.fi/~jviljas/keldysh.pdf

[24] J. Zhu, I. Martin, A. Bishop, Kondo stripes in an Anderson-Heisenberg model of heavy fermion systems, Physical Review letters 100 (23) (2008) 236403.
URL http://link.aps.org/doi/10.1103/PhysRevLett.100.236403

[25] M. Maltseva, M. Dzero, P. Coleman, Electron cotunneling into a Kondo lattice, Physical Review Letters 103 (20) (2009) 206402.
URL http://link.aps.org/doi/10.1103/PhysRevLett.103.206402

[26] P. Wölfle, Y. Dubi, A. V. Balatsky, Tunneling into clean heavy fermion compounds: Origin of the Fano line shape, Physical Review Letters 105 (2010) 246401.
URL http://link.aps.org/doi/10.1103/PhysRevLett.105.246401

[27] A. Schmidt, M. Hamidian, P. Wahl, F. Meier, A. Balatsky, J. Garrett, T. Williams, G. Luke, J. Davis, Imaging the Fano lattice to 'hidden order' transition in URu_2Si_2, Nature 465 (7298) (2010) 570–576.
URL http://dx.doi.org/10.1038/nature09073